A COMPUTATIONAL STUDY ON THE DESIGN OF DONOR-ACCEPTOR COPOLYMERS FOR ORGANIC PHOTOVOLTAIC MATERIALS

by

Birce Kahraman

B.S., Chemistry, Boğaziçi University, 2015

Submitted to the Institute for Graduate Studies in
Science and Engineering in partial fulfillment of
the requirements for the degree of
Master of Science

Graduate Program in Chemistry
Boğaziçi University
2017

ACKNOWLEDGEMENTS

I would first like to thank my thesis advisors Prof. Viktorya Aviyente and Prof. İlknur Doğan for their help and advices.

I would also like to thank the experts who were involved in the validation survey for this research project: Assoc. Prof. Şaron Çatak and Seyhan Salman.

Finally I want to express my gratitude to my family and my boyfriend for their support.

ABSTRACT

A COMPUTATIONAL STUDY ON THE DESIGN OF DONOR-ACCEPTOR COPOLYMERS FOR ORGANIC PHOTOVOLTAIC MATERIALS

Organic solar cells are one kind of renewable energy. In this study, 50 different donor-acceptor oligomers, which were used for photovoltaic materials, were investigated by using 5 different acceptors, which are cyclopentadiphenyl (CPDP), benzodithiophene isomer 1 (BDT1), benzodithiophene isomer 2 (BDT2), cyclopentadithiophene (CPTz), dithienopyridine (DTPn), and 5 different donors, which are benzo[c][1,2,5]thiadiazole (BT), benzo[c][1,2,5]oxadiazole (BX), hydrogentriazole (HTAZ), benzo[c][1,2,5]selenadiazole (BSe), quinoxaline (Qx). Density functional theory (DFT) and time-dependent DFT (TD-DFT) at the B3LYP/6-311G* level have been employed for the calculations. The number of donors increased from 5 to10 by using the heteroatom substitution on the donors. Thus, the effect of heteroatom substitution on optical and geometrical properties of molecules was investigated. Benchmark studies on the methodology were performed to determine HOMO, LUMO energies and optical band gaps of the oligomers. Transition dipole moments, HOMO, LUMO energies and band gaps were calculated as a function of the chain length so, tetramers were found as suitable materials to ensure the energy saturation. Tetramers, which were the optimal chain length, have been used to evaluate the optical and geometrical properties like reorganization energies, distortion energies, frontier molecular orbitals, bond length alternations and excited-state vertical transition energies of oligomers.

In conclusion, suitable photovoltaic materials were designed from a class of oligomers by taking 4 important factors into consideration. The choice of oligomers was based on the following criteria: low reorganization energy, LUMO energy higher than -3.8 eV, HOMO energy range between -5.27 eV and -5.7 eV and the optical band gap between 1.4 eV to 1.9 eV. Overall,16 out of 50 tetramers were found as suitable materials which can be used in solar cells.

ÖZET

ORGANİK FOTOVOLTAİK MATERYALLER İÇİN ALICI-VERİCİ KOPOLİMERLERİN DİZAYNINA YÖNELİK HESAPSAL ÇALIŞMA

Yenilenebilir enerji kaynaklarından biri de güneş panelleridir. Bu çalışmada yoğunluk fonksiyonel teori (DFT) ve B3LYP/6-311G* seviyesindeki zamana bağımlı DFT (TD-DFT) ile 5 farklı alıcı; siklopentadifenil (CPDP), benzoditiyofen izomer 1 (BDT1), benzoditiyofen izomer 2 (BDT2), siklopentaditiyofen (CPTz), ditienopiridin (DTPn) ve 5 farklı verici; benzo[c][1,2,5]tiadiazol (BT), benzo[c][1,2,5]oksadiazol (BX), hidrojentriazol (HTAZ), benzo[c][1,2,5]selenadiazol (BSe), kinoksalin (Qx) kullanılarak fotovoltaik materyaller için kullanılan 50 farklı verici-alıcı oligomer araştırılmıştır. Heteroatom yer değiştirmesi kullanılarak verici sayısı 5 ten 10 a çıkarılmıştır. Böylece moleküle ait geometrik ve optik özellikler üzerindeki heteroatom yer değiştirme etkisi incelenmiştir. Oligomerlerin optik bant aralıkları ve HOMO, LUMO enerjilerini belirlemek için metodoloji üzerine yapılan kıyaslama çalışmaları kullanılmıştır. Geçiş dipol momenleri, HOMO, LUMO enerjileri ve bant aralıkları zincir uzunluğuna bağlı bir fonsiyon olarak hesaplanmıştır, bu şekilde tetramerler enerji doygunluğunu sağlamak açısından en uygun materyaller olarak bulunmuşlardır. En uygun zincir uzunluğuna sahip tetramerler, oligomerlere ait reorganizasyon enerjileri, bozulma enerjileri, hudut orbitalleri, bağ uzunluğu değişimleri ve dikey uyarma enerjileri gibi optik ve geometrik özellikleri değerlendirmek için kullanılmışlardır.

Sonuç olarak, 4 önemli etken dikate alınarak bir sınıf oligomer arasından uygun fotovoltaik materyal seçilmiştir. Bu etkenler düşük reorganizasyon enerjisine, -3.8 eV tan yüksek bir LUMO enerjisine, -5.27 eV ile -5.7 eV aralığında bir HOMO enerjisine ve 1.4 eV ile 1.9 eV aralığında bir bant boşluğuna sahip olmaktır. Bu şekilde, güneş panellerinde kullanılan 50 tetramer arasından 16 tanesi uygun malzeme olarak bulunmuştur.

TABLE OF CONTENTS

LIST OF FIGURES

LIST OF TABLES

LIST OF SYMBOLS

E_c^{VWN}	Vosko-Wilk-Nusair correlation functional
E_x^{exact}	Exact exchange energy
$E_c[\rho]$	Correlation energy
$E_x[\rho]$	Exchange energy
$J[\rho]$	Coulomb energy
$T[\rho]$	Kinetic energy of interacting electrons
$T_s[\rho]$	Kinetic energy of non-interacting electrons
U_x^{σ}	Exchange energy density
$V_{ee}[\rho(\mathbf{r})]$	Interelectronic interactions
$V_{ext}(\mathbf{r})$	External potential
V_{KS}	Kohn-Sham potential
v(r)	External potential
ΔE_x^{B88}	Becke's gradient correction
$\rho(r)$	Electron density
ψ_i	Kohn-Sham orbitals
λ_{ij}	Reorganization Energy
Ψ	Many electron wavefunction

LIST OF ACRONYMS/ABBREVIATIONS

BLA	Bond Length Alternation
B88	Becke 88 Exchange Functional
B3LYP	Becke-3-parameter Lee-Yang-Parr functional
CAM-B3LYP	Coulomb-attenuated Becke-3-parameter Lee-Yang-Parr functional
DFT	Density functional theory
$\hat{H}$	Hamiltonian operator
HOMO	Highest Occupied Molecular Orbital
LDA	Local Density Approximation
LUMO	Lowest Unoccupied Molecular Orbital
M06-2X	Empirical exchange-correlation functional
TD-DFT	Time Dependent Density Functional Theory

1. INTRODUCTION

In the 21st century, the energy sources and how to produce energy became one of the most argued subjects, because the global need of energy is increasing rapidly and energy has to be supplied more to answer this demand. Carbon based fossil fuels are the basic source of energy consumption for today's world, in 2015 the generation of carbon based fossil and nuclear energy was recorded as 76.30% [1]. Some of the reasons for which fossil fuels are chosen as the energy source are that they are cheap, easy to consume, having easy transportation, faster consumption etc. However, besides these benefits, fossil fuels have many negative outcomes. One of the most important problem about using fossil fuels is the carbon dioxide emission. The latter is the primary gas which causes global climate change and air pollution. Due to this reason, many civil organizations and governments arrange campaigns against the use of fossil fuels and the reduction of carbon emission.

Although there are many debates about energy sources and carbon based fossil fuels, the need of energy increases and energy consumption grows by approximately 2% per year. In addition, most of this consumption depends on fossil fuels. If necessary precautions are not taken and fossil fuel consumptions continue, the carbon dioxide emission is going to increase by 30% in 20 years according to the British Petroleum which has an energy outlook about global energy discussion [2]. Another energy source alternative to fossil fuels is nuclear energy. Nuclear energy consumption does not cause a gas emission and it provides more amount of energy with less amount of resource. However, the nuclear energy has many risky points including the radiation caused by nuclear systems which have killed many people over the past years.

The common problem about fossil fuels and nuclear energy is that they are not renewable, which means both are going to have an end one day. To eliminate the previously stated problems and have an endless energy source for increasing demand of human population, renewable energy sources were discovered, namely biofuels, hydroelectric and geothermal systems, wind, wave and solar energy and new technologies. These energy sources have less negative effect on environment and earth as well. Since

they are renewable regardless of the energy consumption, the energy source is almost infinite. However, there are some problems about these resources that need to be improved. For instance, the efficiencies of these systems are not adequate and their set ups are very expensive. In 2015, the amount of total renewable energy generated was as 23.70 % [1]. As it can be seen, the production of renewable energy is not enough to supply the needs.

To be able to increase this production, there is a need of improvements in terms of the cost and efficiency of renewable energies. Solar cells are very important type of renewable energy source and it is safe to say that they are going to be used more in the future. Therefore, the cost and efficiency of solar cells need to be improved for such use and production. For this aspect, some types of solar cells were improved such as inorganic, organic, dye-sensitized and perovskite solar cells.

Inorganic solar cells are the most common types of solar cells due to their high efficiency compared to other types. Some of the most common inorganic solar cell materials are Si, CdTe, and CIGS (copper indium gallium diselenide) [3].

Silicon based solar cells are classified as n-type and p-type. The p-type silicon is obtained by adding atoms such as boron or gallium. Since, the number of valance electrons in boron atom is one less than silicon atom to make a bond, an electron hole forms. The n-type silicon is obtained by adding an atom of phosphorus which has one valance electron more than silicon atom and an unpaired electron moves freely. Although n-type Si solar cells were produced in 1950s, p-type one is common now due to their high resistance to space radiation. In addition, the p-type is more producible and accessible industrially. However, n-type crystalline Si solar cells have higher efficiency by about 20-25 % [4]. The most important drawback of this type is the high production cost and the need of high purity.

CdTe based solar cells are constructed from the thin film of CdTe that absorb sunlight and convert it to electricity. The efficiency of CdTe solar cells is about 13.6 % yet it is still less than of Si solar cells. In addition, CdTe based solar cells are flexible in the surface layer so, this feature provides a significant advantage in terms of higher

power/mass ratio [5]. Although Cd is highly abundant, Te is not. It has a good match with sunlight and lower cost than Si. Another negative outcome of CdTe solar cells is that Cd is a toxic substance.

Another type of common inorganic solar cells is CIGS based solar cells that consist of a substrate such as glass, a back contact such as Mo, an absorber layer such as Cu (In_{1-x}, Ga_x) Se_2, buffer layers such as CdS, InS, ZnS, ZnO and ZnSe, a window layer such as i-ZnO and a TCO layer such as n-ZnO:Al. CIGS thin film solar cells have a lot of advantages such as high absorption of sunlight, band gap of absorber layer which is easy to control and has long term stability. The efficiency of CIGS with the CdS buffer layer is calculated about 19 %, which means they have higher efficiency than CdTe based solar cells. However, cadmium is a very toxic substance; therefore, alternative materials are being searched to use in the absorber layer [6]. Yet the cells made of these materials cannot have as much efficiency as the cells made of Cd and their abundance is not as high as Cd. Also CIGS based solar cells have high fabrication cost as a negative aspect.

Dye-sensitized solar cells (DSSCs) are similar to power conversion devices which generally consist of three parts: a dye-sensitized TiO_2 photoanode, an iodide/triiodide redox electrolyte and a counter electrode [7]. When the photoactive dye is exposed to sunlight, it becomes active and excites electrons by catching photons. Then, the excited electrons are sent to a TiO_2 semiconductor. Thanks to TiO_2, electrons are transmitted to external circuit which is connected to the DSSC. Electrons come back to the dye with the redox reactions via an iodide/triiodide redox electrolyte. DSSCs have many advantages such as low cost materials, simple fabrication processes and high conversion efficiency [7].

Another type of solar cells is perovskite solar cells. The general chemical formula of organic-inorganic metal trihalide perovskite is showed as ABX_3, where A is an organic cation, B is a divalent metal ion, and X is a halide or any combination. Recently, power conversion efficiency of these solar cells is recorded to be greater than 20%. One of their disadvantages is that when perovskite solar cells are exposed to moisture and oxygen, they are degradable. In addition, organic-inorganic perovskites generally contain methyl ammonium lead halide. Despite, their advantages such as easy to fabricate and the strong

solar absorption, lead is highly toxic material therefore, perovskite solar cells should not be used in terms of human health [8].

Although inorganic semiconductors give the better matching with their band gap energies to solar spectrum, the organic materials have higher absorptivities, 2000 times thinner layers and lower cost than inorganic materials. [9] Organic solar cells comprise carbon based compounds that are small molecules, dendrimers and polymers to convert sunlight to electric energy. Organic solar cells have many advantages such as low cost, light weight, long life time and the soluble capability to produce flexible large-area devices [10].

In the literature, there are many types of organic photovoltaic devices such as single layer organic solar cells, multilayer organic solar cells and bulk heterojunction (BHJ) solar cell devices [11]. First, single layer organic solar cells are introduced by adding organic electronic materials such as a small molecule and polymer between two electrodes. Then, multilayer organic cells are produced and an electron rich donor and an electron deficient acceptor are inserted between two electrodes. Their structures are shown in Figure 1.1.

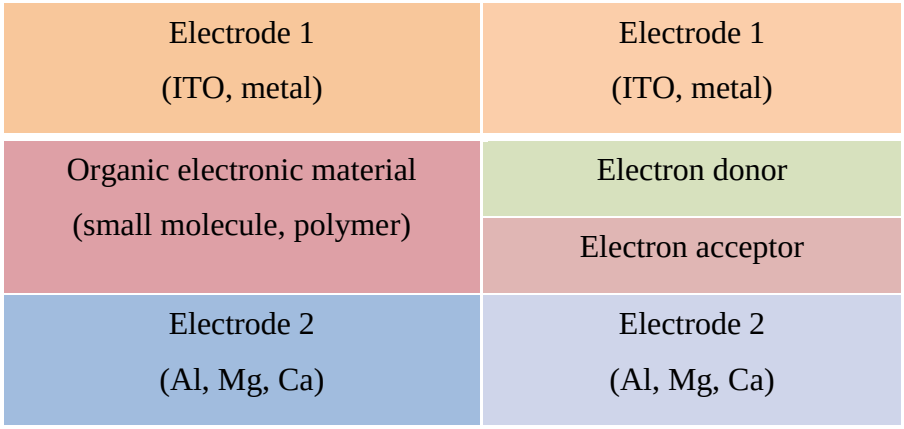

Figure 1.1. Structure of a single layer organic solar cell and a multilayer organic solar cell.

Recently, BHJ solar cell devices are used because of low power conversion efficiency which single layer and multilayer photovoltaic devices have. In a BHJ solar cell, there is an active layer between a transparent anode, typically tin doped indium oxide (ITO) and a metal cathode. A thin layer of poly(3,4-ethylenedioxythiophene)-

poly(styrenesulfonate) (PEDOT:PSS) is inserted in between the ITO and the active layer to increase the electrical contact and arrange energy levels. The active layer consists of two components such as any electron donor as the conjugated polymer and any electron acceptor that generally is used as fullerene derivatives. The structure of BHJ solar cells is shown in Figure 1.2 [12].

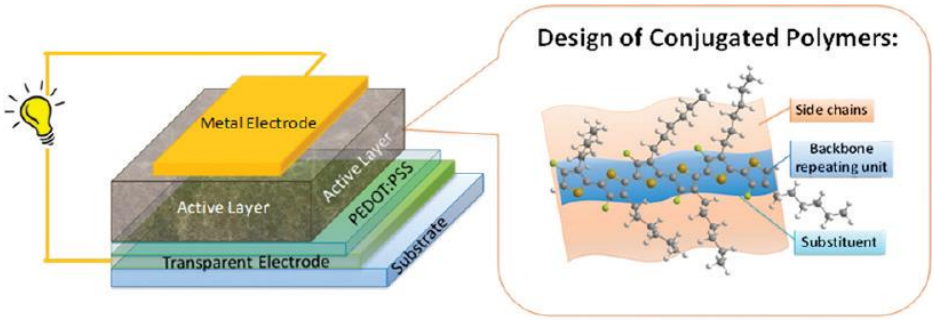

Figure 1.2. Structure of a bulk heterojunction solar cell device [12].

Many donor-acceptor conjugated polymers are used as hole-transport materials in active layer of BHJ organic solar devices to increase the power conversion efficiency. The power conversion efficiency of organic solar cell devices depends on three factors: the open circuit voltage (V_{oc}), the short-circuit current (J_{sc}) and the fill factor (FF). Voc is mainly proportional to the energy level difference between the lowest unoccupied molecular orbital (LUMO) of the acceptor and the highest occupied molecular orbital (HOMO) of the donor. The efficiencies of light absorption of the active layer, exciton diffusion and dissociation in the donor/acceptor interface, the amount of charge transportation in active layer and charge collection on electrodes affect the value of J_{sc}. Finally, FF is related to the series and parallel resistances of instruments [10].

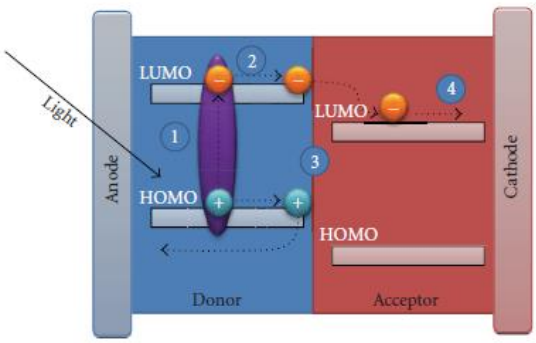

Figure 1.3. Steps of charge transfer mechanism between the anode electrode and the cathode electrode in BHJ solar cells [13].

The charge transfer mechanism in BHJ solar cells is shown in Figure 1.3. This mechanism consists of four steps. In the mechanism, the donor is the hole transporting material which gets in touch with the anode and the acceptor is the electrons transporting material which is in contact with the cathode. The first step is that after photons are absorbed, excitons are formed in the donor material. In the second step of the mechanism, the excitons reach the donor-acceptor interface by diffusing inside the material. Then, as the third step dissociation occurs in the excitons which reach the donor-acceptor interface dissociate. As the fourth and last step, the dissociated excitons continue to diffuse inside the acceptor to be able to reach the cathode electrode. Thus, free charges through the sample, which is used as the acceptor unit, are collected on the cathode electrode [13].

In BHJ organic cells, conjugated polymers that have delocalized electrons of π bonds yield small band gap energies between the HOMO and LUMO. Thus, when these polymers are exposed to low voltage, they conduct electric current by acting like a semiconductor. The reasons why these polymer materials are used are that they have good film-forming properties, strong absorption ability, high hole mobility, reasonable solubility and suitable band gap [14]. Conjugated polymers consist of three components that are the backbone, the side chains and the substituents. The backbone of the polymers affects the physical properties such as energy levels, band gap and inter/intra molecular interaction, the side chains provide an improvement to the molecular weight, solubility and processability. Subsituents such as F or CN are used to tune physical and electronic properties [12]. Therefore, ideal polymers should be designed accordingly.

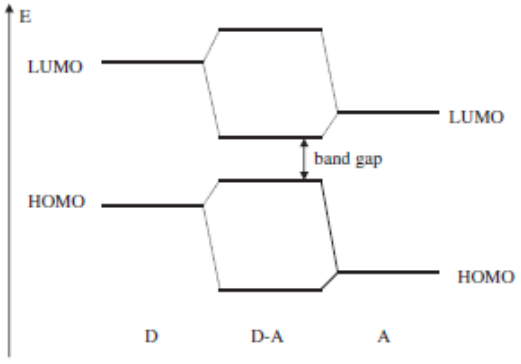

Figure 1.4. Band gaps for donor, acceptor and donor-acceptor conjugated polymers [15].

According to Figure 1.4, the donor normally has higher HOMO and LUMO levels than the acceptor. However, when donor-acceptor conjugated polymers are used in solar cells, the HOMO level of donor and the LUMO level of acceptor are close so the band gap is lower. The presence of electron donating groups (EDG) such as thiophene or pyrrole on the donor and electron withdrawing groups such as CN, NO_2, quinoxalines, pyrazines or thiadiazole on the acceptor, causes intra-chain charge transfer from the donor to the acceptor [15].

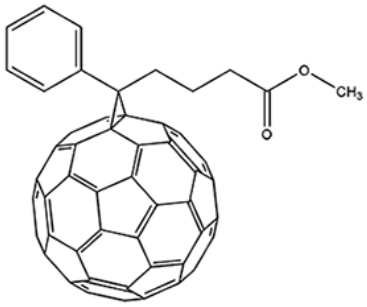

Figure 1.5. Chemical structure of [6,6]-phenyl-C61-butyric acid methyl ester (PCBM) [16].

In BHJ solar cells, the materials used for the acceptor are fullerene derivatives such as C_{60}, [6,6]-$PC_{61}BM$, PCBG, $BTPF_{60}$, C_{70}, [6,6]-$PC_{71}BM$ and $BTPF_{70}$. [6,6]-phenyl-C_{61}-butyric acid methyl ester, PCBM, is one of the common materials used for organic photovoltatics because of better electron transport (Figure 1.5). In addition, PCBM has an important role which is interaction between the high molecular weight materials of high regioregularity and low molecular weight materials of low regioregularity [15]. Conjugated polymers, oligomers or small molecules such as diketopyrrolo[3,4-c] pyrrole (DPP) [17], polythiophenes [18], polyfluorenes [19], oligothiophenes [20], acenes and fused polycycles [21] are given as some examples of donor materials.

Modeling is a very important part of chemistry for academic improvements. Thanks to modeling, more data can be collected with less effort and many predictions can be made without experiments. These benefits let us to save economic sources and time.

2. AIM OF THE STUDY

Solar cells are one kind of renewable energies. In this study, the design of donor-acceptor copolymers for photovoltaic materials is purposed by investigating electronic, geometrical and optical properties of a certain class of donor oligomers that are used in bulk heterojunction solar cells. Five donors, which are cyclopentadiphenyl (CPDP), benzodithiophene isomer 1 (BDT1), benzodithiophene isomer 2 (BDT2), cyclopentadithiophene (CPTz), dithienopyridine (DTPn), and five acceptors, which are benzo[c][1,2,5]thiadiazole (BT), benzo[c][1,2,5]oxadiazole (BX), hydrogentriazole (HTAZ), benzo[c][1,2,5]selenadiazole (BSe), quinoxaline (Qx), are chosen in this study. Si and N heteroatom substitutions are carried out in the donors of CPDP and CPTz and Si heteroatom substitution in the donor of DTPn so, the number of donors increases. 10 different donors and 5 different acceptors make 50 molecules in total. In addition, their geometric and optical properties such as reorganization energies, distortion energies, bond length alternation, frontier molecular orbitals and vertical excitation energies and the effect of heteroatom substitution on optical and geometrical properties of oligomers are investigated.

Overall, in this study a suitable computation method to discriminate oligomers for organic photovoltaic cells is proposed.

3. METHODOLOGY

3.1. Density Functional Theory

Density Functional Theory (DFT) is [22] defined as a quantum mechanical approach. Kohn-Hohenberg theorem says that to be able to determine the wavefunction, it is enough to have the ground state density. By using the theorem, DFT gives an opportunity to calculate the electronic structure of atoms and molecules [23, 24].

This theory includes several theorems. One of them is about the relation between the electron density $\rho(\mathbf{r})$ and the external potential $V_{ext}(\mathbf{r})$. According to this theorem, the potential of the nuclei depends on the electron density. The variation principle is also stated in another theorem, where it says that the calculation of the electron density is variable according to many aspects such as the wavefunction, position of nuclei and energy [22, 25].

The electron density is defined as:

$$\rho(x) = N \int \cdots \int |\Psi(x_1, x_2, \cdots, x_n)|^2 dx_1 dx_2 \cdots dx_n \tag{3.1}$$

where x represents both spin and spatial coordinates of electrons.

The electronic energy can be represented as a function of the electron density:

$$E[\rho] = \int v(r)\rho(r)dr + T[\rho] + V_{ee}[\rho] \tag{3.2}$$

where $T[\rho]$ is the kinetic energy of the interacting electrons and $V_{ee}[\rho]$ is the electronic interaction energy. The electronic energy is expressed as

$$E[\rho] = \int v(r)\rho(r)dr + T_s[\rho] + J[\rho] + E_{xc}[\rho] \tag{3.3}$$

The coulomb energy is $J[\rho]$, the kinetic energy of the non-interacting electrons is $T_s[\rho]$ and the exchange-correlation functional energy is $E_{xc}[\rho]$ which is the sum of an exchange functional $E_x[\rho]$ and a correlation functional $E_c[\rho]$. However, $E_{xc}[\rho]$ may include a kinetic energy difference between the interacting and non-interacting electronic systems. The favorable electron-electron repulsion energy contributions are the measure of the freedom which is the kinetic energy term and the change of opposite spin electrons which is the exchange-correlation energy. On the other hand, the unfavorable energy which disfavors the total electronic energy is described by the Coulomb energy [26].

Kohn-Sham density functional theory is an imaginary theory, where a set of independent reference orbitals ψ_i satisfy the particle independent Schrödinger equation. According to Kohn-Sham, one-body V_{KS} yields the same density with the real fully-interacting system in a reference system of independent non-interacting electrons.

$$\left[-\frac{1}{2}\nabla^2 + V_{KS}\right]\psi_i = \varepsilon_i\psi_i \tag{3.4}$$

The one-body potential V_{KS} is defined as

$$V_{KS} = v(r) + \frac{\partial J[\rho]}{\partial \rho(r)} + \frac{\partial E_{xc}[\rho]}{\partial \rho(r)} \tag{3.5}$$

$$V_{KS} = v(r) + \frac{\rho(r')}{|r - r'|}dr' + v_{xc}(r) \tag{3.6}$$

where $v_{xc}(r)$ is the exchange-correlation potential. The independent orbitals ψ_i are known as Kohn-Sham orbitals and give the exact density by

$$\rho(r) = \sum_i^N |\psi_i|^2 \tag{3.7}$$

if the exact form of the exchange-correlation functional is known. However, there is a need to have approximate forms developed from the local density approximation (LDA), because the exact form of this functional is not known. The energy of a uniform electron

gas is calculated by this approximation. As an example, a large number of electrons in uniformly distributed positive charged system make it neutral. The energy expression is

$$E[\rho] = T_s[\rho] + \int \rho(r) v(r) dr + J[\rho] + E_{xc}[\rho] + E_b \tag{3.8}$$

where E_b is the electrostatic energy of the positive background. Since the positive charge density is equal with the negative charge density due to uniform electron distribution of particles, the energy expression is reduced to

$$E[\rho] = T_s[\rho] + E_{xc}[\rho] \tag{3.9}$$

$$E[\rho] = T_s[\rho] + E_x[\rho] + E_c[\rho] \tag{3.10}$$

The kinetic energy functional can be described as

$$T_s[\rho] = C_F \int \rho(r)^{5/3} dr \tag{3.11}$$

where C_F is a constant equal to 2.8712. The exchange functional is given as

$$E_x[\rho] = -C_x \int \rho(r)^{4/3} dr \tag{3.12}$$

where C_x is a constant equal to 0.7386. The parametrization of the results of a set of quantum Monte Carlo calculations gives the correlation energy, $E_c[\rho]$, for a homogeneous electron gas.

The LDA method cannot give the exact results of the exchange energy and decreases these results by about 10 percent. Therefore, correct asymptotic behavior cannot be observed. To be able to have this asymptotic behavior of exchange energy density, any finite many-electrons system is calculated as,

$$\lim_{x\to\infty} U_x^{\sigma} = -\frac{1}{r} \tag{3.13}$$

U_x^{σ} is related to $E_x[\rho]$ by

$$E_x[\rho] = \frac{1}{2}\sum_{\sigma}\int \rho_{\sigma} U_x^{\sigma} dr \tag{3.14}$$

A gradient-corrected functional is proposed by Becke

$$E_x = E_x^{LDA} - \beta\sum_{\sigma}\int \rho_{\sigma}^{4/3} \frac{x_{\sigma}^2}{1+6\beta x_{\sigma}\sinh^{-1} x_{\sigma}} dr \tag{3.15}$$

where σ symbolizes the electron spin, $x_{\sigma} = \frac{|\nabla\rho_{\sigma}|}{\rho_{\sigma}^{4/3}}$ and β is an empirical constant (β=0.0042). This functional is known as Becke88 (B88) functional [24].

The non-interacting Kohn-Sham reference system (λ=0) is connected to the fully-interacting real system (λ=1) by the adiabatic connection formula, which is

$$E_{xc} = \int_0^1 U_{xc}^{\lambda} d\lambda \tag{3.16}$$

where λ is the interelectronic coupling-strength parameter and U_{xc}^{λ} is the potential energy of exchange-correlation at intermediate coupling strength. The adiabatic connection formula can be approximated by

$$E_{xc} = \frac{1}{2}E_x^{exact} + \frac{1}{2}U_{xc}^{LDA} \tag{3.17}$$

since, $U_{xc}^{0} = E_x^{exact}$, which is the exact exchange energy of the Slater determinant of the Kohn-Sham orbitals, and $U_{xc}^{1} = U_{xc}^{LDA}$ [21].

The closed shell Lee-Yang-Parr (LYP) correlation functional [28] is described by

$$E_c = -a\int \frac{1}{1+d\rho^{-1/3}}\left\{\rho + b\rho^{-2/3}\left[C_F\rho^{5/3} - 2t_w + (\frac{1}{9}t_w + \frac{1}{18}\nabla^2\rho)\right]e^{-c\rho^{-1/3}}\right\}dr \quad (3.18)$$

where

$$t_w = \frac{1}{8}\frac{|\nabla\rho(r)|^2}{\rho(r)} - \frac{1}{8}\nabla^2\rho \quad (3.19)$$

The hybrid functionals consist of LDA, B88, E_x^{exact} and the gradient-corrected correlation functional [28] which includes three parameters.

$$E_{xc} = E_{xc}^{LDA} + a_0\left(E_x^{exact} - E_x^{LDA}\right) + a_x\Delta E_x^{B88} + a_c\Delta E_c^{non-local} \quad (3.20)$$

where ΔE_x^{B88} is the Becke's gradient correction of the exchange functional. In the B3LYP functional, there is the gradient-correction ($\Delta E_c^{non-local}$) of the correlation functional in LYP. However, there is also a local correlation term which must be added to the correction term only in LYP.

$$\Delta E_c^{non-local} = E_c^{LYP} - E_c^{VWN} \quad (3.21)$$

E_c^{VWN} is the Vosko-Wilk-Nusair correlation functional, which is parametrized form of the LDA correlation energy according to Monte Carlo calculations. The empirical coefficients are a_0=0.20, a_x=0.72 and a_c=0.81 [29].

3.2. Time Dependent Density Functional Theory

To be able to calculate the electronic excited states, a quantum mechanical approach named Time Dependent Functional Theory (TD-DFT) can be used. The Hamiltonian Operator is described as

$$\hat{H} = \hat{T}(\underline{r}) + \hat{W}(\underline{r}) + \hat{V}_{ext}(\underline{r}, t) \tag{3.22}$$

The kinetic energy of the electrons is denoted by $\hat{T}(\underline{r})$, the coulomb interactions between the electrons are denoted by $\hat{W}(\underline{r})$, and the influence of time-dependent potential on the electrons is denoted by $\hat{V}_{ext}(\underline{r}, t)$. The external potential determines the excited state. Therefore, when calculating the properties of the excited state, the potential effects must be known.

To a variational principle involving the action

$$A = \int_{t_0}^{t_1} \langle \Psi(t) | i\frac{\partial}{\partial_t} - \hat{H} | \Psi(t) \rangle \, dt \tag{3.23}$$

the Hohenberg-Kohn Theorem is applied and the wavefunction is determined up to a time-dependent constant

$$\Psi(\boldsymbol{r}_1, \dots, \boldsymbol{r}_N, t) = \Psi[\rho](t) e^{-i\alpha(t)} \tag{3.24}$$

The phase factor is added as a constant to the action in Equation 3.23:

$$A[\rho] = \int_{t_0}^{t_1} \langle \widetilde{\Psi}[\rho](t) | i\frac{\partial}{\partial_t} - \hat{H}(t) | \widetilde{\Psi}[\rho](t) \rangle \, dt + \alpha(t_1) - \alpha(t_0) = A[\rho] + const. \tag{3.25}$$

and A[ρ] can be written as

$$A[\rho] = B[\rho] - \int d\boldsymbol{r} \int_{t_0}^{t_1} (\boldsymbol{r}, t) \rho(\boldsymbol{r}, t) dt \tag{3.26}$$

where B[ρ] is independent of the external potential. Assume an independent system which has the property described in Equation 3.27:

$$\rho(\boldsymbol{r}, t) = \sum_i f_i |\Psi_i(\boldsymbol{r}, t)|^2 \tag{3.27}$$

Hence to rewrite B[ρ],

$$B[\rho] = \sum_i f_i \int_{t_0}^{t_1} \langle \Psi_i(t) | i\frac{\partial}{\partial_t} - \frac{1}{2}\nabla_i^2 | \Psi_i(t) \rangle \, dtv - \frac{1}{2}\int_{t_0}^{t_1} dt \iint d\mathbf{r}_1 d\mathbf{r}_2 \frac{\rho(\mathbf{r}_1,t)\rho(\mathbf{r}_2,t)}{|\mathbf{r}_1 - \mathbf{r}_2|} - A_{xc}[\rho] \tag{3.28}$$

In which, the exchange and correlation are denoted by $A_{xc}[\rho]$. Applying the variational principle to (3.27) with constraint

$$\rho(\boldsymbol{r},t) = \sum_i f_i|\Psi_i(\boldsymbol{r},t)|^2 = \sum_i^N |\Psi_i(\boldsymbol{r},t)|^2 \tag{3.29}$$

we obtain the time-dependent Kohn-Sham Equation in Equation 3.30:

$$\left[-\frac{1}{2}\nabla^2 + v_{eff}(\boldsymbol{r},t)\right]\Psi_i(\boldsymbol{r},t) = i\frac{\partial}{\partial_t}\Psi_i(\boldsymbol{r},t) \tag{3.30}$$

$$v_{eff}(\boldsymbol{r},t) = v_H(\boldsymbol{r},t) + v_{xc}(\boldsymbol{r},t) + v_{ext}(\boldsymbol{r},t) \tag{3.31}$$

the time-dependent exchange potential is unknown in this equation, and all exchange and correlation effects in TD-DFT are collected in Equation 3.32.

$$v_{xc}(\boldsymbol{r},t) = \frac{\delta A_{xc}[\rho]}{\delta\rho(\boldsymbol{r},t)} \tag{3.32}$$

Since time-dependent density functional theory equations are exact, approximations are not needed. On the other hand, some approximations are needed for the exchange correlation functional, because the exchange correlation functional is not known exactly.

The adiabatic approximation (AA) is shown in Equation 3.33:

$$v_{xc}[\rho](\boldsymbol{r},t) = \frac{\delta A_{xc}[\rho]}{\delta\rho(\boldsymbol{r},t)} \approx \frac{\delta E_{xc}[\rho]}{\delta\rho(\boldsymbol{r})}\Big|_{\rho=\rho(\boldsymbol{r},t)} \tag{3.33}$$

The change in electron densities results in the exchange and correlation potential change.

3.3. Reorganization Energies

Charge transport in organic materials may occur in two different ways; hopping-type and band-type [30]. Hopping-type charge transfer occurs in π-conjugated molecules. On the geometry of the oligomers internal arrangements take place with the movement of electrons between oligomers. To determine the charge transfer properties of organic materials, internal reorganizations, which control the charge transfer mobility, have an essential role as a parameter. The reorganization energy depends on the conjugation length

and degree [31].

By the addition or removal of electrons, the alterations in the geometry of a molecule occur and result in a change in energy named inner reorganization energy. The conformation and energy changes of ionic state of the molecule and the energy of addition or removal of an electron in neutral conformation should be known to be able to calculate the inner reorganization energy.

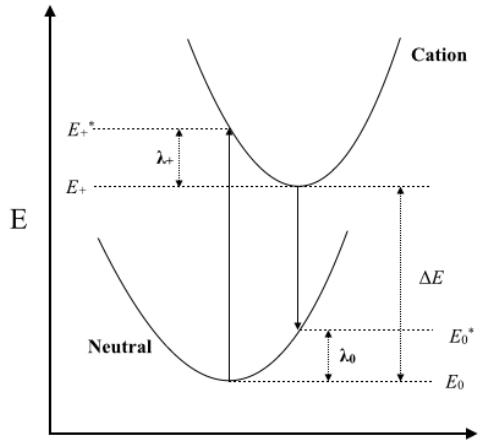

Figure 3.1. Internal reorganization energy $\lambda_+ + \lambda_0$ for hole transfer, and adiabatic ionization energy, ΔE.

In the equation of the reorganization energy λ_+ refers to the difference between the energy needed to change the conformation from neutral to cation state (E_+^*) and the total energy of the cation (E_+). λ_0 refers to the difference between the needed energy to change the geometry from cation to neutral state (E_0^*) and the total energy of the neutral (E_0). The hole transfer reorganization energy (λ) can be calculated by the sum of two components which are $\lambda_0$and λ_+. The summary of these calculations is shown in equation 3.34.

$$\lambda = \lambda_0 + \lambda_+ = (E_0^* - E_0) + (E_+^* - E_+) \tag{3.34}$$

A similar calculation is needed to calculate the electron transfer reorganization. The λ_- part refers to the difference between the needed energy to change the conformation from

neutral to anion state (E_{-}^{*}) and the total energy of the anion (E_{-}). λ_0 part of it refers to the difference between the needed energy to change the geometry from anion to neutral state (E_0^{*}) and the energy of the neutral (E_0). The electron transfer reorganization energy is calculated by the summation of two components which are λ_0 and λ_{-}. Equation 3.35 is a brief summary, and Figure 3.2 is a graphical illustration of this calculation.

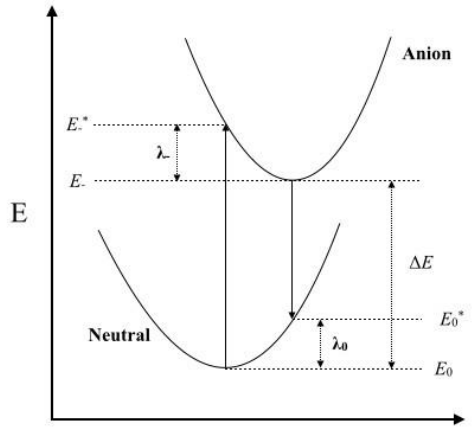

$$\lambda = \lambda_0 + \lambda_{-} = (E_0^{*} - E_0) + (E_{-}^{*} - E_{-}) \quad (3.35)$$

Figure 3.2. Internal reorganization energy λ-+ λ0 for electron transfer, and adiabatic ionization energy, ΔE.

3.4. Geometrical Properties

3.4.1. Distortion Energies

Distortion energy is an important parameter to determine the planarity of the polymer. It is calculated as the total energy difference between the relaxed geometry and the constrained conformation which has dihedral angles between the donor and the acceptor constrained to zero. The neutral oligomers are optimized and the dihedral angles of this neutral conformation are monitored. Then, the dihedral angles of the relaxed geometry are constrained to zero thus, the constrained geometry is obtained [32]. Finally, single point calculations are performed. The distortion energy is an important factor to analyze the effect of steric hindrance between the donor and the acceptor.

3.4.2. Bond Length Alternation

Bond length alternation is a geometrical parameter which presents a measure of conjugation in molecular structures. The average bond length alternation is calculated as the difference between the lengths of a single bond and the adjacent multiple bond such as double or triple bond in π-delocalized systems [33].

In the literature, there are the relationships between the bond length alternation and the conductance of molecular wires, the charge transport properties of the oligomers, as well as the band gap of the oligomers, the linear polarizability, α, the second-order polarizability, β, and the third-order polarizability, γ [34]. In this study, relationships between the bond length alternation and charge transport properties of the oligomers are investigated.

Bond length alternations are calculated for oligomers which consist of the donors of X/CPDP, BDT1 and BDT2. The oligomers containing the donor of X/CPTz and Y/DTPn do not have the C-C bond in the π-conjugation path of the donor therefore, the bond length alternations of these oligomers are not calculated.

3.5. Benchmark Calculations

The methodology is an important factor which affects the obtained results; therefore, the suitable methodology is determined by a study where the HOMO and LUMO energies and also optical and fundamental band gaps are calculated. Following Seferos et al. [35], there are five different computational models to use at the B3LYP/6-311G* level of the theory. In Model 1, the geometries are optimized at the neutral singlet ground state thus, the HOMO energies and the LUMO energies are calculated. Then, the difference between the HOMO energies and the LUMO energies are calculated and fundamental band gaps are obtained. The neutral singlet geometry of Model 1 is used for all other models. In Model 2, Model 3 and Model 4 single point calculations are performed on oxidized (+1) doublet; reduced (-1) doublet and the neutral triplet states. In Model 5, the vertical excitation energies to the lowest lying excited states are calculated by using TD-DFT calculations from the neutral singlet state.

The band gaps of the oligomers are obtained with two different ways. The first one is calculating the fundamental band gaps by using the energy differences between the HOMO and the LUMO from the optimized neutral singlet state (Model 1). The second one is obtaining the vertical excitation energy of lowest lying singlet excited state ($S_0 \rightarrow S_1$) by using the TD-DFT calculations (Model 5).

The HOMO energies are calculated in two different ways. The first one is obtaining the HOMO energies at the optimized neutral singlet state (Model 1). The second one is obtaining the HOMO energies by using the energy differences between optical band gaps (E_{opt}) from the TD-DFT calculations and αHOMO energies from the neutral triplet state. In this model, the HOMO energies are calculated by the energy differences between the vertical excitation energies from Model 5 and αHOMO energies from Model 4.

The LUMO energies are evaluated in two different ways. The first one is obtaining LUMO energies at the optimized neutral singlet state (Model 1). The second one is calculating the LUMO energies by using the αHOMO energy at the neutral triplet state (Model 4).

4. RESULTS AND DISCUSSION

4.1. Determination of the Methodology

4.1.1. The Effect of Side Chain

Copolymers that have 2,1,3-benzothiadiazole (BT) as the acceptor unit and dithienopyridine (DTPn) or cyclopentadithiophene (CPDT) as the donor units with side chains are used to understand the effect of side chain. Calculations were performed with the B3LYP/6-31G* methodology and all calculations were performed by using Gaussian09 (Revision E.01) software package.

In Table 4.1, the calculated HOMO-LUMO energy gaps are shown as 2.94 eV for PDTPn-BT and 2.53 eV for PCPDTBT. To analyze the effect of side chains on the band gaps of oligomers, n-octyl and 2-ethylhexyl side chains were replaced with hydrogen atoms. The energy difference between the monomer with side chains and the monomer without side chains was small. As we can observe from Table 4.1, the effect of side chains on band gaps was negligible. However the calculated values were not still good enough and did not get close to the experimental values which were 1.4 and 2.1 eV [12].

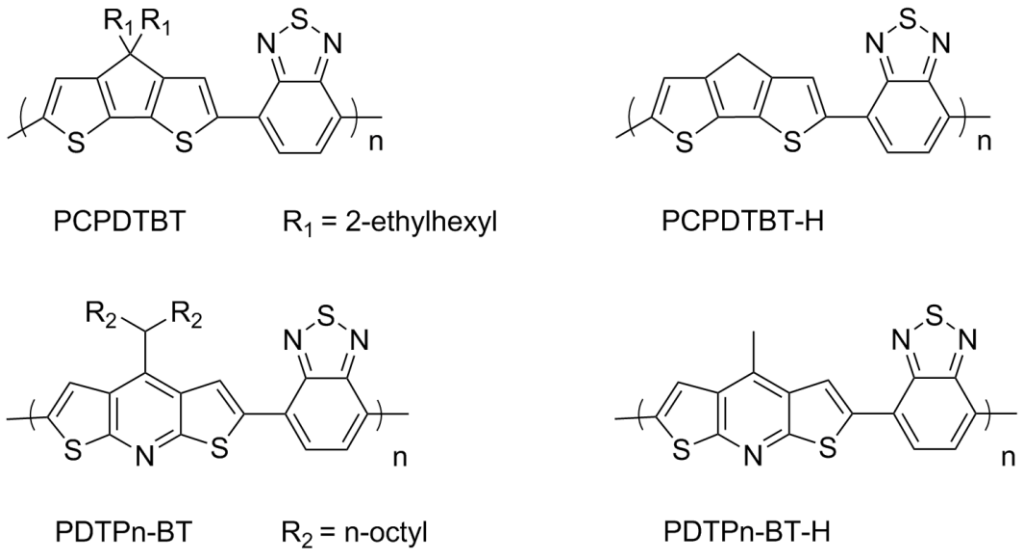

Figure 4.1. Chemical structures of the oligomers chosen for benchmark calculations.

Table 4.1. HOMO, LUMO levels and fundamental band gaps for benchmark calculations (B3LYP/6-31G*).

Polymer	HOMO (eV)	LUMO (eV)	ΔE (eV)	Experimental HOMO (eV)	Experimental ΔE (eV)
PCPDTBT	-4.89	-2.36	2.53	-5.3	1.4
PCPDTBT-H	-4.90	-2.34	2.55		
PDTPnBT	-5.73	-2.79	2.94	-5.6	2.1
PDTPn-BT-H	-5.54	-2.53	3.01		

4.1.2. Choice of the DFT Functional

The calculated results of band gaps in Table 4.1 were not close to the experimental values hence the optical band gaps of PCPDTBT-H copolymer with different DFT functionals (M06-2X, B3LYP and CAM-B3LYP) were calculated by using the time-dependent density functional theory (TD-DFT). According to the obtained data of optical band gaps in Table 4.2, the B3LYP functional gave better results than the others. Also, when larger basis sets were used, the change in the optical band gaps was negligible as it can be seen in Table 4.2, therefore, the method of B3LYP with the 6-311G* basis set is chosen for all subsequent calculations. We can observe that the band gaps with TD-DFT were smaller than the ones in the ground state in Table 4.1. However, a result which is similar to the experimental value (1.4 eV) was not observed thus, the change of their optical band gaps was investigated by increasing the number of repeating unit (n) up to 4.

Table 4.2. Calculated optical band gaps (ΔE) from TD-DFT calculations with different methods and basis sets and experimental band gap for a molecule without side chains.

Polymer	Method	ΔE (eV)	Experimental ΔE (eV)
PCPDTBT-H	M06-2X/6-31G*	2.84	1.4
	B3LYP/6-31G*	2.23	
	CAM-B3LY/6-31G*	2.90	
	B3LYP/6-311G*	2.23	
	CAM-B3LY/6-311G*	2.95	

4.1.3. Determination of Chain Length

To observe the effect of the chain length of the oligomers, calculations were performed by increasing the chain lengths. In Table 4.3, the symbol n represents the number of the repeating unit. It has been assessed that as the number of repeating units increases, in PCPDTBT-H and PDTPn-BT-H molecules, the optical band gaps decreased and both showed the best result for the tetramers. For example, the optical band gap of the oligomer of PCPDTBT-H was calculated as 1.39 eV for tetramers and the experimental band gap of the oligomer of PCPDTBT-H was 1.4 eV. The difference between the experimental value and the calculated value was 0.01 eV and was negligible. Therefore, the suitable method was chosen as TD-DFT at the B3LYP/6-311G* level for tetramers.

Table 4.3. Calculated HOMO-LUMO energy gaps, optical band gaps from TD-DFT calculations versus the number of repeating units (n) (B3LYP/6-311G*).

Oligomers	n	ΔE (eV)	Optical Band Gap (eV)	Experimental ΔE (eV)
PCPDTBT-H	1	2.55	2.23	1.4
	2	2.25	1.73	
	3	2.19	1.51	
	4	1.64	1.39	
PDTPn-BT-H	1	3.01	2.57	2.1
	2	2.79	2.19	
	3	2.82	2.11	
	4	2.39	2.06	

HOMO and LUMO energies of the molecules were evaluated as a function of the number of the repeating units (n) and are displayed in Figure 4.2. There is a relationship between the inverse number of the repeating units and the HOMO or LUMO energies. As you can see in Figure 4.2, the HOMO energies of the molecules increased and the LUMO energies of the molecules decreased with an increasing number of the repeating unit. Therefore, the band gap energies of the molecules are expected to decrease. The HOMO energy difference between trimers and tetramers was smaller than the HOMO energy

difference between trimers and dimers so, energy saturation was obtained after tetramers. The same trend was observed for the LUMO energy difference between trimers and tetramers. Transition dipole moments of the molecules have a linear slope with the chain length in Figure 4.3 thus, accuracy about the energy saturation are obtained. Chains which are longer than tetramers could be ignored thanks to the energy saturation in HOMO and LUMO levels so, accuracy was provided by gaining computational time.

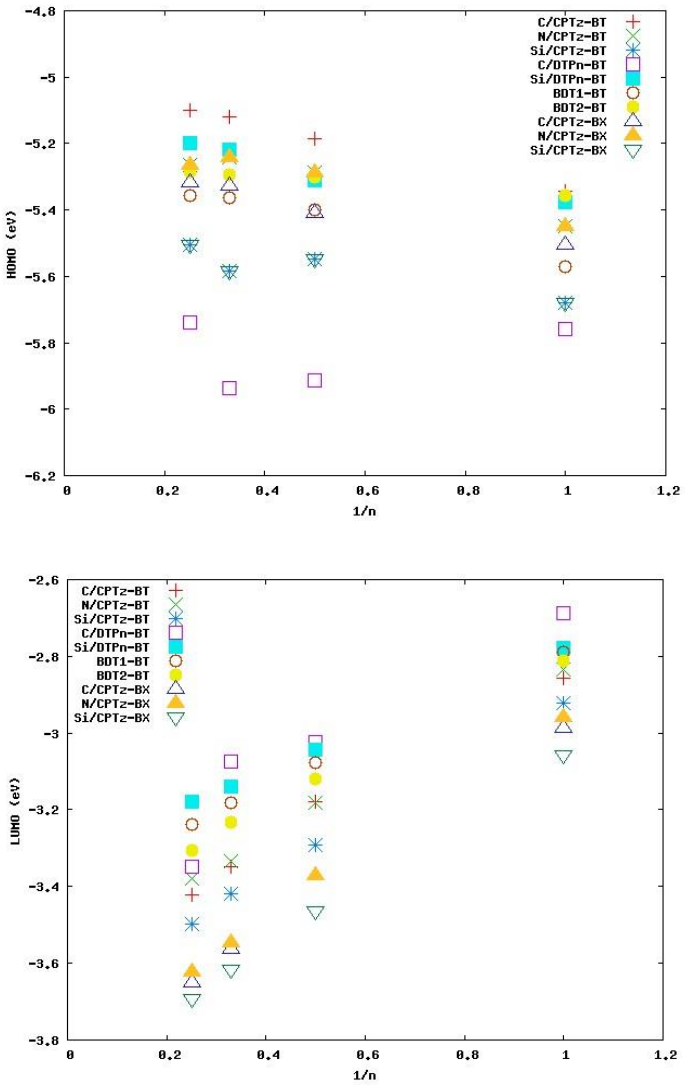

Figure 4.2. HOMO and LUMO energies as a function of chain length (B3LYP/6-311G*).

Figure 4.3 shows the transition dipole moment for the $S_0 \rightarrow S_1$ vertical transition and optical band gap energies as a function of the number of repeating units. Transition dipole moments increase and optical band gap energies decrease with an increase of the

chain length. High transition dipole moments are desired for photovoltaic materials because films which have high absorptivity can be obtained and more photons are captured with materials which have high transition dipole moments [36]. The molecules which have the CPTz donor showed higher transition dipole moments than the others. The molecules which have the BT acceptor have lower transition dipole moments compared to the BX acceptor. Optical band gap energies for pentamers are shown in Figure 4.3. The energy difference between tetramers and pentamers was negligible therefore, chains which are longer than tetramers have not been considered for further studies.

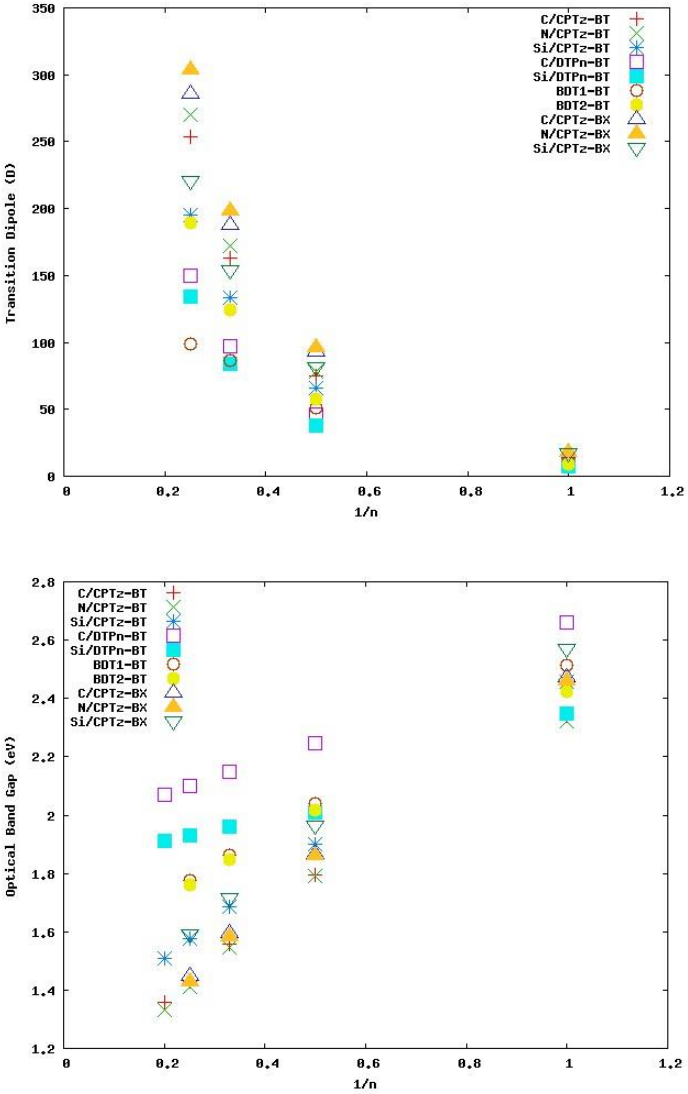

Figure 4.3. Transition dipole moment and optical band gap as a function of chain length (B3LYP/6-311G*).

4.2. Determination of the Conformation

In this study, five donors and five acceptors were chosen to be examined. The donors were cyclopentadiphenyl (CPDP), benzodithiophene isomer 1 (BDT1), benzodithiophene isomer 2 (BDT2), cyclopentadithiophene (CPTz), dithienopyridine (DTPn). CH_2, SiH_2 and NH were used for X in CPDP and CPTz to have three different donors in each case, CH and SiH were replaced with Y in DTPn to have two different donors as well. The acceptors were benzo[c][1,2,5]thiadiazole (BT), benzo[c][1,2,5]oxadiazole (BX), hydrogentriazole (HTAZ), benzo[c][1,2,5]selenadiazole (BSe), quinoxaline (Qx). All combinations of donor-acceptor couples were examined (Figure 4.4). In the donors of CPDP, CPTz and DTPn the heteroatom was changed. There are 10 different donors and 5 different acceptors that make 50 molecules in total.

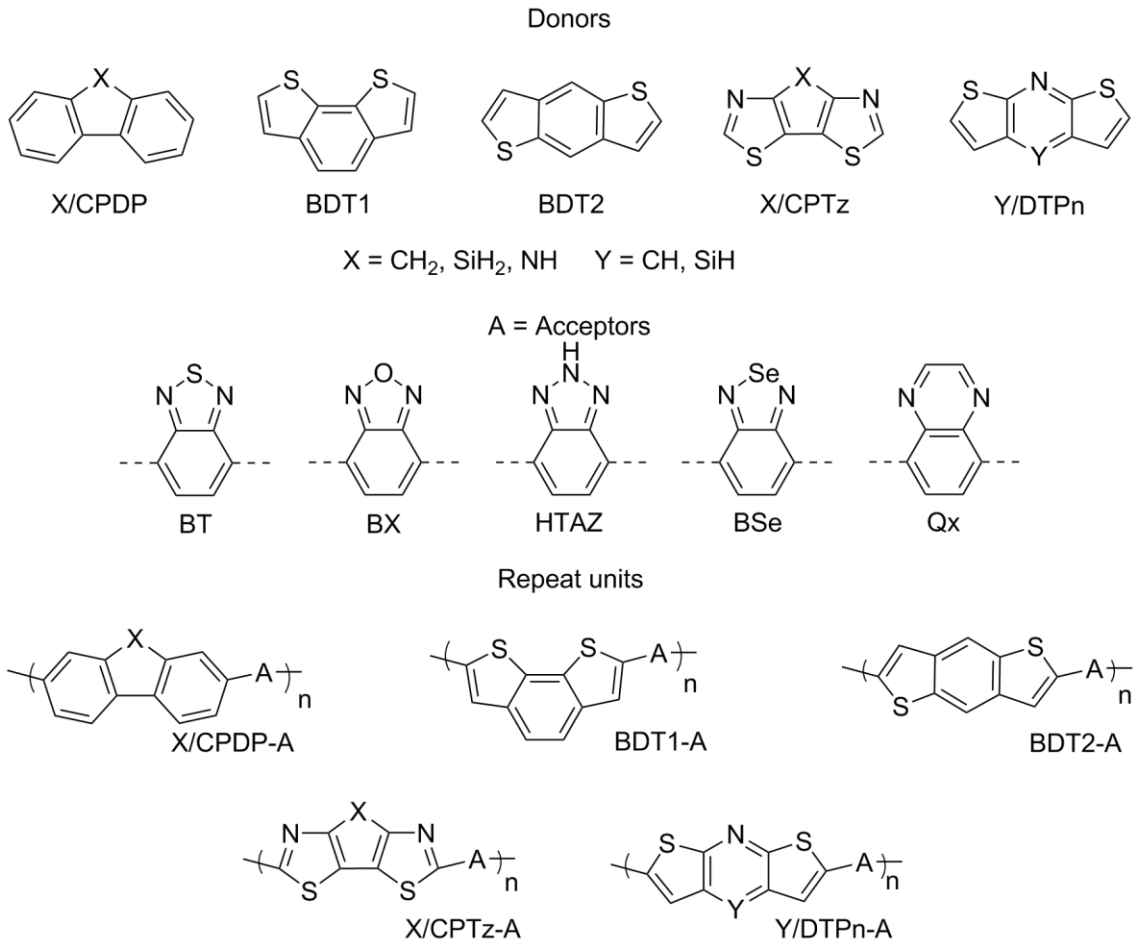

Figure 4.4.Chemical structures of the donors, acceptors and copolymer repeating units.

The conformation search was done on these oligomeric chain systems. The positions of the donor and acceptor fragments were evaluated according to *syn* or *anti* conformations. The conformation in which electronegative atoms of donors and acceptors stay in the same direction is described as *syn* conformation (dd or uu), and opposite direction is described as *anti* (ud or du).

For the D-A system a thorough search was made for the dimer systems with 8 different possible conformations. In this study, it was seen that all the donors except X/CPDP, showed the lowest energy at the conformation du/du. Thus, the trimers and tetramers were designed according to the best result of the dimers. Tetramers have the conformation du/du/du/du. In the case of X/CPDP, dd/du was the most favored conformation for the dimer, which was upgraded to a tetramer as dd/du/dd/du. As shown in Table 4.4 the conformation of the *anti* (du) was the best result for the monomer of C/DTPn-BT and the conformation of the *anti-anti* (du-du) was the best result for the dimer of C/DTPn-BT in Table 4.5. Therefore, the best conformation of tetramers was designed as *anti-anti-anti-anti* (du/du/du/du).

Table 4.4. Calculated relative energies (kcal/mol) for monomers of C/DTPn-BT with different conformations (B3LYP/6-311G*).

Name	Conf.	E_{rel}
C/DTPn-BT	du (*anti*)	0
	dd (*syn*)	1.98

Table 4.5. Calculated relative energies (kcal/mol) for dimers of C/DTPn-BT with different conformations (B3LYP/6-311G*).

Name	Conf.	E_{rel}
C/DTPn-BT	dudu (*anti-anti*)	0
	dudd (*anti-syn*)	1.70
	duuu (*anti-syn*)	3.53
	duud (*anti-anti*)	1.52
	uuuu (*syn-syn*)	5.18
	dduu (*syn-syn*)	3.56
	ddud (*syn-anti*)	1.49
	dddu (*syn-anti*)	3.48

4.3. Distortion Energies

Figure 4.5 displays the dihedral angles of the oligomers studied. When X/CPDP was compared to the other donors, the derivatives of X/CPDP indicate large deviations from the planar backbone. Large deviations of X/CPDP might be caused by steric hindrance between the hydrogen atoms on the donor ring and the neighbor atoms of the acceptor. The atomic sizes of selenium and sulfur atoms are quite large in comparison with the atomic sizes of nitrogen and oxygen atoms. However, the highest torsion angles (44^{o}) were seen in the acceptor of Qx containing nitrogen atoms. The reason of high torsion angles might be the interaction between the donor of CPDP and acceptors since the molecules containing the donor of CPDP showed high torsion angles as well as large deviations on the molecular geometry. Deviations on the molecular geometry because of high torsion angles can be affect the delocalization of the planar backbone so, the planarity of molecules is lost and the intramolecular charge transfer can be affected. D-A systems including Qx, BSe and BT acceptors show distortion energy around 52.0, 21.0 and 26.5 kcal/mol but the donor materials except for CPDP indicated smaller deviations of the torsion angles and their distortion energies were less than 2.1 kcal/mol. In this study, the distortion energies for all the copolymers are reported in Table 4.6.

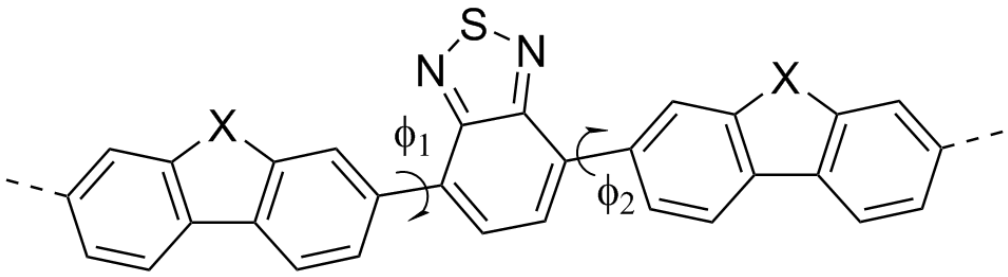

Figure 4.5. Dihedral angles of donor-acceptor oligomers.

Table 4.6. Torsion angles (°) along the conjugated backbone and total energy difference (kcal/mol) between constrained coplanar conformations and full relaxed geometries (B3LYP/6-311G*).

Tetramers	Φ_1	Φ_2	ΔE_{tot}
C/CPTz-BT	0	0	0
N/CPTz-BT	0	0	0
Si/CPTz-BT	0	0	0
C/DTPn-BT	0	0	0
Si/DTPn-BT	0	0	0
BDT1-BT	1	1	0
BDT2-BT	0	0	0
C/CPDP-BT	38	38	21.3
N/CPDP-BT	37	37	21.2
Si/CPDP-BT	37	37	20.9
C/CPTz-BX	0	0	0
N/CPTz-BX	0	0	0
Si/CPTz-BX	0	0	0
C/DTPn-BX	0	0	0
Si/DTPn-BX	1	1	0
BDT1-BX	0	0	0
BDT2-BX	0	0	0
C/CPDP-BX	31	31	9.9
N/CPDP-BX	31	30	10
Si/CPDP-BX	31	31	9.7
C/CPTz-Bse	0	0	0
N/CPTz-Bse	0	0	0
Si/CPTz-BSe	0	0	0
C/DTPn-BSe	0	0	0
Si/DTPn-BSe	2	2	0
BDT1-BSe	4	4	0.1
BDT2-BSe	0	0	0
C/CPDP-Bse	38	38	26.6
N/CPDP-Bse	38	38	26.9
Si/CPDP-Bse	39	38	26.2
C/CPTz-HTAZ	0	0	0
N/CPTz-HTAZ	0	0	0
Si/CPTz-HTAZ	0	0	0
C/DTPn-HTAZ	0	0	0
Si/DTPn-HTAZ	1	0	0
BDT1-HTAZ	1	1	0
BDT2-HTAZ	0	0	0
C/CPDP-HTAZ	33	32	11.8

Table 4.6. Torsion angles (°) along the conjugated backbone and total energy difference (kcal/mol) between constrained coplanar conformations and full relaxed geometries (B3LYP/6-311G*). (cont.)

Tetramers	**Φ_1**	**Φ_2**	**ΔE_{tot}**
N/CPDP-HTAZ	33	32	12.1
Si/CPDP-HTAZ	33	33	11.4
C/CPTz-Qx	0	0	0
N/CPTz-Qx	0	0	0
Si/CPTz-Qx	0	0	0
C/DTPn-Qx	22	22	2.1
Si/DTPn-Qx	20	18	1.6
BDT1-Qx	21	22	2
BDT2-Qx	20	20	1.8
C/CPDP-Qx	44	44	52.8
N/CPDP-Qx	44	44	52.1
Si/CPDP-Qx	44	44	52.1

4.4.Bond Length Alternation

Calculations of the bond length alternation are only performed for the donors of BDT1, BDT2, CPDP and their derivatives and are shown in Table 4.7. The donors of CPTz and DTPn do not contain the C-C bond in the π-conjugation path of the donor. Therefore, the bond length alternation for these donors was not calculated. Although the acceptor of BSE had the highest value of BLA (0.048 Å) than others, the acceptor of HTAZ showed the lowest result (0.031 Å). However, significant differences between the values of bond length alternation of donors were not observed.

Table 4.7. Bond length alternations (Å) of several oligomers.

Donor-Acceptor				
BLA				
	BT	BX	BSe	HTAZ
C/CPDP	0.042	0.042	0.045	0.039
N/CPDP	0.034	0.034	0.036	0.031
Si/CPDP	0.045	0.045	0.048	0.042
BDT1	0.040	0.040	0.042	0.039
BDT2	0.039	0.040	0.041	0.034

4.5. Reorganization Energies

Reorganization energy is an important factor to determine the properties of charge transfer and charge mobility in photovoltaic materials. When compounds have smaller reorganization energy, these compounds show higher charge transfer rate and higher charge mobility. If the length of conjugation path along the backbone increases, the reorganization energies for holes and electrons decrease [37]. In Table 4.8, reorganization energies for holes (λ_{Hole}) and electrons ($\lambda_{Electron}$), adiabatic ionization potential (AIP), adiabatic electron affinity (AEA), vertical ionization potential (VIP), vertical electron affinity (VEA) energies are given for all molecules.

In Table 4.8, the compounds that contain the X/CPTz donor moieties show the highest reorganization energies for holes and electrons. The λ_{Hole} values are found in the range of 161 meV to 203 meV. When the effect of heteroatom on the reorganization energies of these compounds was examined, N/CPTz molecules showed smaller λ_{Hole} values than Si/CPTz and C/CPTz molecules. According to the λ_{Hole} results of C/CPTz and Si/CPTz molecules, the energy difference between two molecules was minimal about 6 meV. When X/CPTz donors were combined with the Qx acceptor fragments, the lowest λ_{Hole} values are found for X/CPTz donor moieties. The results of λ_{Hole} values for BDT1 and BDT2 changed between 4 meV and 8 meV with the exception of the molecule of BDT1-Qx. BDT2 molecules showed lower λ_{Hole} values than BDT1 molecules. However, the effect of the presence of the thiophene ring on BDT1 and BDT2 was negligible. X/DTPn moieties had the lowest λ_{Hole} values within all compounds. According to the heteroatom effect (C vs. Si) in X/DTPn, the significant energy differences of 31-38 meV were found in the λ_{Hole} values of Si/DTPn molecules when compared with the C/DTPn molecules. Si/DTPn moieties showed the lowest λ_{Hole} values in all investigated molecules and are found in the range of 58 meV to 64 meV. Thus, low λ_{Hole} values of Si/DTPn are suitable for the intramolecular hole transport. X/CDPD moieties indicate similar results with the acceptor fragments. Si/CDPD-BSe had the highest λ_{Hole} value as 140 meV and C/CPDP-Qx had the lowest λ_{Hole} value as 125.38 meV when compared with other acceptor fragments.

Table 4.8. Reorganization energies (meV), adiabatic ionization potential (AIP), adiabatic electron affinity (AEA), vertical ionization potential (VIP), vertical electron affinity (VEA) (ev) energies of DA oligomers (B3LYP/6-311G*).

Compounds	λ_{Hole}	$\lambda_{Electron}$	AIP	AEA	VIP	VEA
C/CPTz-BT	191.75	122.50	5.66	-2.81	5.75	-2.75
N/CPTz-BT	179.39	124.04	5.60	-2.78	5.68	-2.72
Si/CPTz-BT	186.61	112.16	5.91	-2.87	6.00	-2.81
C/DTPn-BT	97.76	64.65	6.29	-2.58	6.34	-2.55
Si/DTPn-BT	62.15	55.39	5.95	-2.48	5.98	-2.45
BDT1-BT	117.57	75.38	5.87	-2.53	5.93	-2.49
BDT2-BT	111.14	79.64	5.85	-2.59	5.91	-2.55
C/CPDP-BT	133.08	106.46	6.01	-2.08	6.08	-2.03
N/CPDP-BT	132.56	112.84	5.97	-2.05	6.04	-2.00
Si/CPDP-BT	131.18	105.09	6.15	-2.18	6.22	-2.13
C/CPTz-BX	199.46	146.87	5.89	-3.04	5.98	-2.97
N/CPTz-BX	186.49	147.60	5.83	-3.02	5.92	-2.95
Si/CPTz-BX	193.75	133.37	6.13	-3.08	6.22	-3.01
C/DTPn-BX	101.16	75.45	6.51	-2.75	6.55	-2.71
Si/DTPn-BX	63.92	63.47	6.14	-2.64	6.17	-2.61
BDT1-BX	120.80	90.25	6.11	-2.75	6.16	-2.70
BDT2-BX	112.11	95.87	6.06	-2.79	6.11	-2.74
C/CPDP-BX	130.47	137.79	6.17	-2.29	6.24	-2.22
N/CPDP-BX	133.84	139.51	6.13	-2.26	6.19	-2.19
Si/CPDP-BX	139.18	148.10	6.31	-2.41	6.37	-2.33
C/CPTz-BSe	203.45	62.10	5.56	-2.85	5.66	-2.80
N/CPTz-BSe	190.13	119.54	5.50	-2.82	5.59	-2.77
Si/CPTz-BSe	199.45	106.06	5.82	-2.91	5.91	-2.86
C/DTPn-BSe	97.87	61.11	6.21	-2.64	6.26	-2.61
Si/DTPn-BSe	64.23	53.55	5.89	-2.54	5.92	-2.51
BDT1-BSe	120.92	70.72	5.80	-2.58	5.86	-2.55
BDT2-BSe	115.19	73.40	5.79	-2.64	5.84	-2.61
C/CPDP-BSe	129.13	87.84	5.96	-2.15	6.03	-2.10
N/CPDP-BSe	134.24	95.39	5.92	-2.12	5.98	-2.08
Si/CPDP-BSe	140.00	97.30	6.09	-2.24	6.16	-2.19
C/CPTz-HTAZ	180.33	146.68	5.55	-2.43	5.64	-2.36
N/CPTz-HTAZ	168.45	147.78	5.49	-2.38	5.57	-2.31
Si/CPTz-HTAZ	180.88	135.53	5.81	-2.51	5.89	-2.44
C/DTPn-HTAZ	91.24	78.93	6.15	-2.13	6.20	-2.09
Si/DTPn-HTAZ	61.06	65.84	5.83	-2.08	5.86	-2.04
BDT1-HTAZ	112.94	95.51	5.72	-2.06	5.78	-2.01
BDT2-HTAZ	108.43	102.02	5.72	-2.16	5.77	-2.11
C/CPDP-HTAZ	127.69	173.94	5.82	-1.58	5.89	-1.49

Table 4.8. Reorganization energies (meV), adiabatic ionization potential (AIP), adiabatic electron affinity (AEA), vertical ionization potential (VIP), vertical electron affinity (VEA) (ev) energies of DA oligomers (B3LYP/6-311G*). (cont.)

Compounds	λ_{Hole}	$\lambda_{Electron}$	AIP	AEA	VIP	VEA
N/CPDP-HTAZ	131.60	185.49	5.78	-1.53	5.85	-1.44
Si/CPDP-HTAZ	135.17	183.20	5.96	-1.73	6.03	-1.64
C/CPTz-Qx	170.65	120.33	5.58	-2.54	5.66	-2.48
N/CPTz-Qx	161.22	123.64	5.51	-2.50	5.59	-2.44
Si/CPTz-Qx	174.64	112.15	5.84	-2.61	5.92	-2.56
C/DTPn-Qx	157.39	147.24	6.26	-2.27	6.32	-2.20
Si/DTPn-Qx	57.59	109.57	5.86	-2.20	5.89	-2.15
BDT1-Qx	148.59	166.02	5.82	-2.21	5.89	-2.11
BDT2-Qx	109.58	170.29	5.80	-2.29	5.86	-2.20
C/CPDP-Qx	125.38	109.27	6.02	-1.69	6.08	-1.64
N/CPDP-Qx	125.69	120.18	5.97	-1.66	6.03	-1.60
Si/CPDP-Qx	135.71	121.61	6.15	-1.80	6.22	-1.74

4.6. Frontier Molecular Orbitals

One of important factors which increases the power conversion efficiency is the effective absorption of photons in the visible region [38]. Therefore, energies of $S_0 \rightarrow S_1$ transitions should be calculated accurately. In Table 4.9, vertical transition energies (E_{vert}, wavelengths (λ), oscillator strengths (*f*) of electronic excitations and electronic configurations are reported.

Compounds with the X/CPDP donor have the lowest oscillator strengths. Similarly, compounds with the BDT1 donor have lower oscillator strength than the others. The heteroatom effect on the donor moieties did not change the results of the oscillator strength extremely. When compared with the effect of heteroatom on the acceptor fragments, the highest oscillator strengths with the HTAZ acceptor fragments were reported. Within all compounds, BDT-BSe and N/CPDP-BSe compounds showed the lowest oscillator strengths (*f*=1.44).The reason of the lowest oscillator strengths could be the steric hindrance because selenium and silicon atoms have bulky size as compared to oxygen and nitrogen atoms.

According to the literature, the most suitable optical band gap energies range is 1.4 eV to 1.9 eV [39, 40]. Vertical excitation energies of oligomers with the X/CPTz donor are found in the desired region. However, there were two exceptions in this donor class which are C/CPTz-BSe and N/CPTz-BSe. The effect of C/N heteroatom did not affect the optical band gaps significantly. However, the C/Si heteroatom change on the CPTz donor changed the optical band gaps by about 0.2 eV. In case of the DTPn donor, the compound of Si/DTPn-BSe was only shown in the suitable optical band gap region. Silicon atom on the DTPn donor might destabilize the HOMO of the donor. Compounds with the BDT1 and BDT2 donors showed their optical band gaps in the desired region except for the BSe and Qx containing systems. Furthermore, the molecules which include the donor of X/CPDP could not fit in the expected region. This could be the result of the high electron affinity or the higher LUMO energies of the X/CPDP as compared to the other donor materials. The optical band gap of the X/CPDP was shown to be between 2.20 eV to 2.77 eV.

Table 4.9. TD-DFT results for all the molecules investigated (B3LYP/6-311G*).

Compounds	**E_{vert} (eV)**	**λ (nm)**	***f***	**Electronic configuration**
C/CPTz-BT	1.43	867	3.50	HOMO → LUMO (96%)
N/CPTz-BT	1.41	879	3.68	HOMO → LUMO (96%)
Si/CPTz-BT	1.58	787	2.97	HOMO → LUMO (94%)
C/DTPn-BT	2.10	591	3.03	HOMO → LUMO (76%)
Si/DTPn-BT	1.93	642	2.50	HOMO → LUMO+2 (50%)
BDT1-BT	1.78	698	1.70	HOMO → LUMO (92%)
BDT2-BT	1.76	703	3.22	HOMO → LUMO (92%)
C/CPDP-BT	2.35	527	1.94	HOMO → LUMO (80%)
N/CPDP-BT	2.34	530	1.90	HOMO → LUMO (71%)
Si/CPDP-BT	2.41	515	2.24	HOMO → LUMO (83%)
C/CPTz-BX	1.45	855	3.99	HOMO → LUMO (96%)
N/CPTz-BX	1.43	867	4.19	HOMO → LUMO (97%)
Si/CPTz-BX	1.59	778	3.38	HOMO → LUMO (95%)
C/DTPn-BX	2.15	578	3.50	HOMO → LUMO (67%)
Si/DTPn-BX	1.98	625	3.03	HOMO → LUMO+2 (44%)
BDT1-BX	1.80	690	2.10	HOMO → LUMO (92%)
BDT2-BX	1.78	697	3.68	HOMO → LUMO (92%)
C/CPDP-BX	2.32	535	2.71	HOMO → LUMO (78%)
N/CPDP-BX	2.30	539	2.51	HOMO → LUMO (72%)
Si/CPDP-BX	2.36	525	3.00	HOMO → LUMO (81%)
C/CPTz-Bse	1.31	945	3.08	HOMO → LUMO (95%)
N/CPTz-Bse	1.29	958	3.26	HOMO → LUMO (96%)

Table 4.9. TD-DFT results for all the molecules investigated (B3LYP/6-311G*). (cont.)

Compounds	E_{vert} (eV)	λ (nm)	*f*	Electronic configuration
Si/CPTz-BSe	1.46	851	2.62	HOMO → LUMO (93%)
C/DTPn-BSe	1.97	631	2.55	HOMO → LUMO (75%)
Si/DTPn-BSe	1.80	689	2.08	HOMO → LUMO+2 (51%)
BDT1-BSe	1.66	746	1.44	HOMO → LUMO (91%)
BDT2-BSe	1.65	751	2.84	HOMO → LUMO (91%)
C/CPDP-Bse	2.23	556	1.56	HOMO → LUMO (78%)
N/CPDP-Bse	2.20	562	1.44	HOMO → LUMO (70%)
Si/CPDP-Bse	2.29	540	1.75	HOMO → LUMO (80%)
C/CPTz-HTAZ	1.68	736	4.42	HOMO → LUMO (96%)
N/CPTz-HTAZ	1.68	740	4.69	HOMO → LUMO (96%)
Si/CPTz-HTAZ	1.82	683	3.72	HOMO → LUMO (94%)
C/DTPn-HTAZ	2.42	513	4.32	HOMO → LUMO (85%)
Si/DTPn-HTAZ	2.31	536	4.79	HOMO-2 → LUMO (32%)
BDT1-HTAZ	2.08	595	2.48	HOMO → LUMO (93%)
BDT2-HTAZ	2.06	602	4.47	HOMO → LUMO (94%)
C/CPDP-HTAZ	2.68	463	3.57	HOMO → LUMO (88%)
N/CPDP-HTAZ	2.70	459	3.48	HOMO → LUMO (86%)
Si/CPDP-HTAZ	2.70	460	3.90	HOMO → LUMO (88%)
C/CPTz-Qx	1.57	789	3.43	HOMO → LUMO (94%)
N/CPTz-Qx	1.56	797	3.61	HOMO → LUMO (95%)
Si/CPTz-Qx	1.72	722	2.98	HOMO → LUMO (92%)
C/DTPn-Qx	2.39	518	3.13	HOMO → LUMO (63%)
Si/DTPn-Qx	2.15	577	2.26	HOMO → LUMO (46%)
BDT1-Qx	2.07	598	1.50	HOMO → LUMO (89%)
BDT2-Qx	2.03	611	2.98	HOMO → LUMO (89%)
C/CPDP-Qx	2.71	457	1.80	HOMO → LUMO (77%)
N/CPDP-Qx	2.70	460	1.66	HOMO → LUMO (73%)
Si/CPDP-Qx	2.77	448	2.08	HOMO → LUMO (79%)

HOMO and LUMO energies are important parameters to evaluate the short circuit voltage (J_{sc}) and the open circuit voltage (V_{oc}) to increase the power conversion efficiency. In the literature, the air oxidation threshold is known as -5.27 eV [41] therefore, HOMO energies of photovoltaic materials should be lower than -5.27 eV. In addition, energy differences between HOMO-HOMO levels of the donors and the acceptors and LUMO-LUMO levels of the donors and the acceptors should be at least 0.3 eV to ensure effective charge separation [42]. In the literature, $PC_{61}BM$, which is commonly used in bulk heterojunction cells, is chosen as an electron acceptor material with its HOMO energy -6.0 eV and LUMO energy -4.1 eV [43].

The calculated HOMO energies were evaluated according to the value of the air oxidation threshold and suitable energy differences between HOMO levels of the donors and HOMO level of the acceptors, which is -6.0 eV, so the $^{+}$ boxes in Table 4.10 is chosen according to the suitable HOMO energy range. The * boxes are chosen according to the common part of both the LUMO energies in Table 4.11 and optical band gaps in Table 4.12 and showed common parts.

In addition, the graph of HOMO energies of all $^{+}$ and * data versus all donors is shown in Figure 4.6. The nomenclature used in Figure 4.6, Figure 4.7 and Figure 4.8 is given below.

1. C/CPTz
2. N/CPTz
3. Si/CPTz
4. C/DTPn
5. Si/DTPn
6. BDT1
7. BDT2
8. C/CPDP
9. N/CPDP
10. Si/CPDP

Table 4.10. Calculated HOMO energies by using the energy difference between optical band gaps from Model 5 and αHOMO energies from Model 4 (B3LYP/6-311G*)

Donor - Acceptor					
	BT	BX	BSe	HTAZ	QX
C/CPTz	-5.41*	-5.69*	-5.32^{+}	-5.34*	-5.28*
N/CPTz	-5.34*	-5.63*	-5.25^{+}	-5.27*	-5.22*
Si/CPTz	-5.65*	-5.92	-5.57*	-5.59*	-4.95*
C/DTPn	-5.43^{+}	-6.50	-6.09	-6.14	-6.10
Si/DTPn	-5.81	-6.12	-5.73	-5.88	-5.38^{+}
BDT1	-5.61*	-5.90	-5.54*	-5.52^{+}	-5.51^{+}
BDT2	-5.62*	-5.88	-5.44*	-5.55^{+}	-5.46^{+}
C/CPDP	-5.89	-6.16	-5.9	-5.76	-5.79
N/CPDP	-5.52^{+}	-6.05	-5.83	-5.75	-5.72^{+}
Si/CPDP	-6.07	-6.33	-6.07	-5.92	-6.00

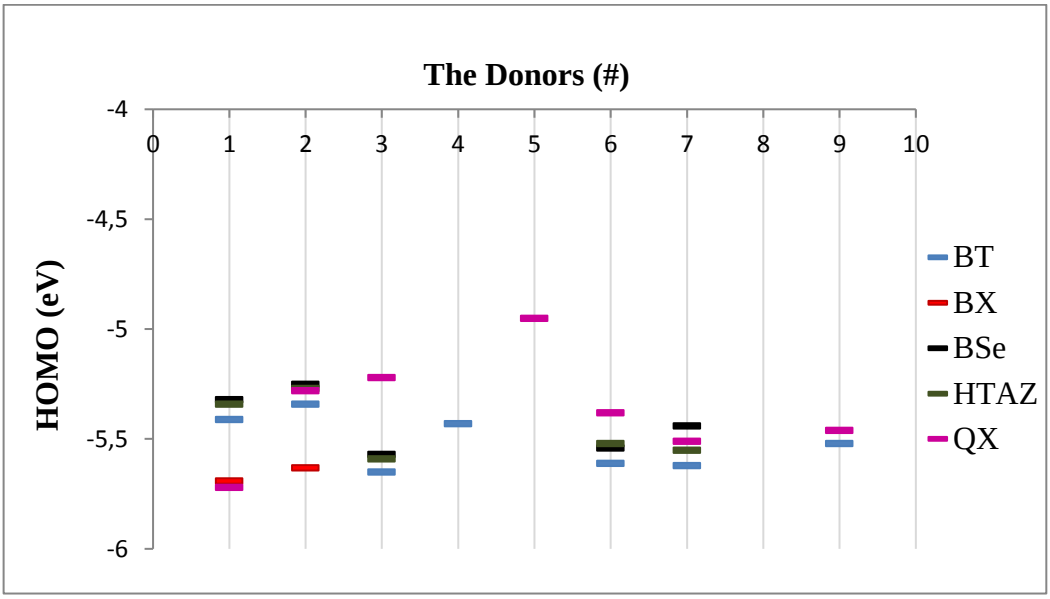

Figure 4.6. Calculated HOMO energies versus donors (B3LYP/6-311G*).

Calculated LUMO energies from Model 1 are shown in Table 4.11 and are chosen according to the suitable energy differences between the LUMO levels of the donors and LUMO level of the acceptor which is -4.1 eV. All LUMO levels of oligomers are suitable for photovoltaic materials. However, the * boxes in Table 4.11 are chosen according to the suitable HOMO levels and optical band gap range. In addition, the graph of LUMO energies of all molecules versus all donors is shown in Figure 4.7.

Table 4.11. Calculated LUMO energies from Model 1 (B3LYP/6-311G*).

Donor - Acceptor					
	BT	BX	BSe	HTAZ	Qx
C/CPTz	-3.42*	-3.65*	-3.45	-2.97*	-3.01*
N/CPTz	-3.38*	-3.62*	-3.42	-2.96*	-3.24*
Si/CPTz	-3.50*	-3.69	-3.42*	-3.12*	-3.30*
C/DTPn	-3.35	-3.57	-3.27	-2.77	-2.91
Si/DTPn	-3.18	-3.36	-3.16	-2.69	-2.96
BDT1	-3.24*	-3.40	-3.22*	-2.70	-3.00
BDT2	-3.30*	-3.41	-3.26*	-2.81	-2.84
C/CPDP	-2.90	-3.22	-2.93	-2.45	-2.58
N/CPDP	-2.91	-3.21	-2.93	-2.43	-2.83
Si/CPDP	-3.03	-3.30	-3.00	-2.56	-2.81

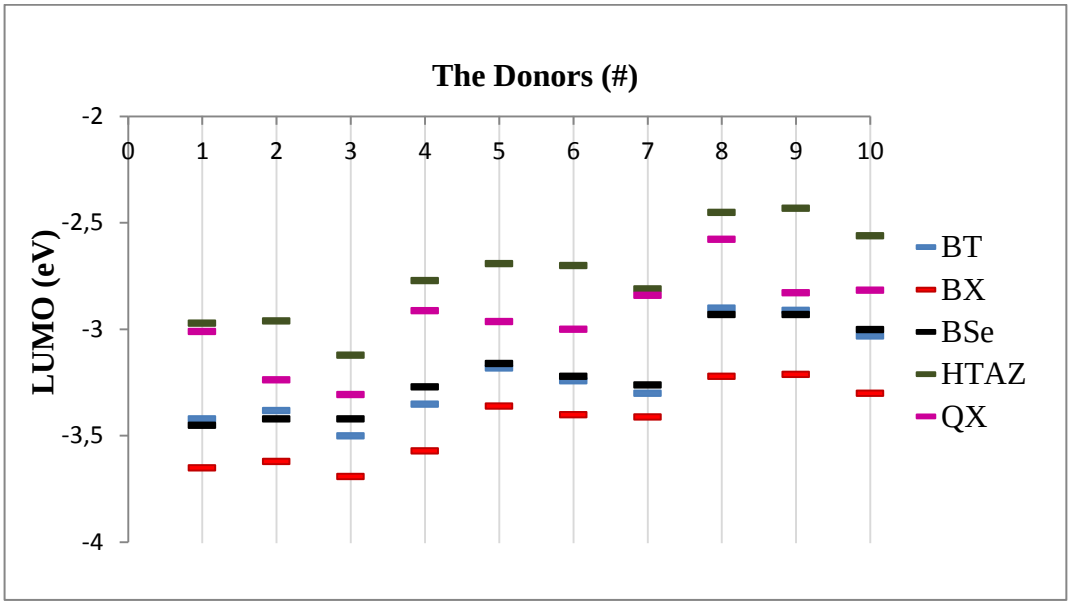

Figure 4.7. Calculated LUMO energies versus donors (B3LYP/6-311G*).

Calculated optical band gaps from Model 5 are shown in Table 4.12 and are chosen according to the suitable optical band gap range which is between 1.4 eV to 1.9 eV. * and $^{+}$ parts showed suitable optical band gap energies for photovoltaic materials. However, the * boxes are more important than the other because they contain suitable HOMO and LUMO energy levels. In addition, the graph of suitable optical band gap energies versus all donors is shown in Figure 4.8

Table 4.12. Calculated optical band gaps of the copolymers from Model 5 (B3LYP/6-311G*).

Donor - Acceptor					
	BT	BX	BSe	HTAZ	QX
C/CPTz	1.43*	1.45*	1.31	1.68*	1.57*
N/CPTz	1.41*	1.43*	1.29	1.68*	1.56*
Si/CPTz	1.58*	1.59^{+}	1.46*	1.82*	1.72*
C/DTPn	2.10	2.15	1.97	2.42	2.39
Si/DTPn	1.93	1.98	1.80^{+}	2.31	2.15
BDT1	1.78*	1.80^{+}	1.66*	2.08	2.07
BDT2	1.76*	1.78^{+}	1.65*	2.06	2.03
C/CPDP	2.35	2.32	2.23	2.68	2.71
N/CPDP	2.34	2.30	2.20	2.70	2.70
Si/CPDP	2.41	2.36	2.29	2.70	2.77

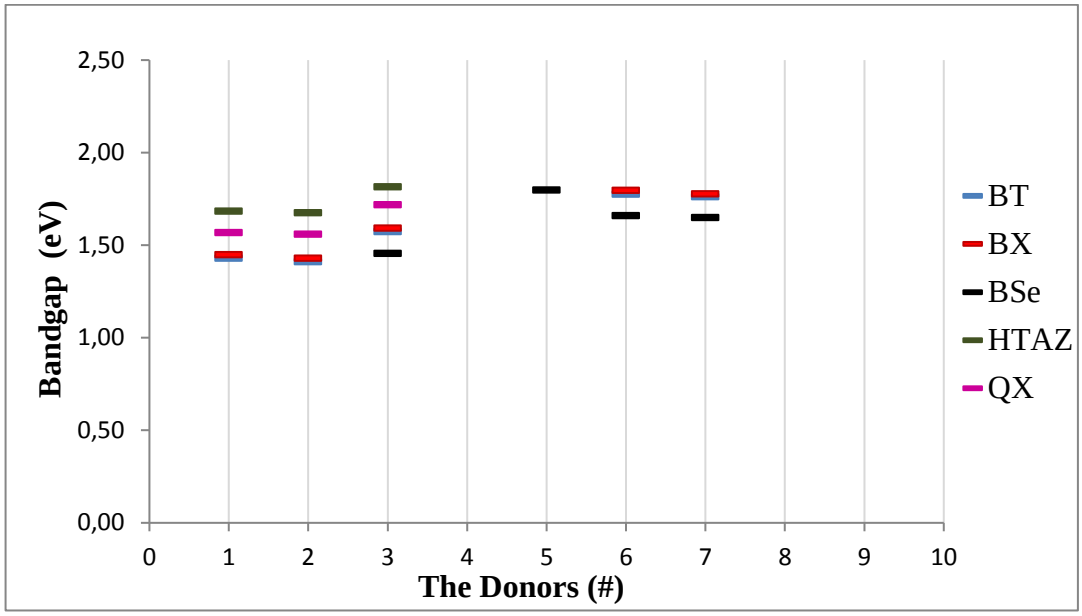

Figure 4.8. Calculated optical band gaps of copolymers versus donors (B3LYP/6-311G*).

4.7. HOMO and LUMO Wave Function Distributions

HOMO and LUMO wave function distributions of all molecules are shown in Figure 4.9. $S_0 \rightarrow S_1$ excitations were observed from HOMO to LUMO transitions. The HOMO wave functions in the DA oligomers are delocalized over both donor and acceptor fragments for all the molecules. However, the LUMO wave functions show two types of localizations which are over the acceptor fragment or over both the donor slightly and the acceptor components. The LUMO wave functions of oligomers which have the donor of CPTz, its derivatives, the acceptor of HTAZ and its derivatives are delocalized over both the donor and acceptor components. When the heteroatom in D-A oligomers was substituted, the LUMO wave functions show the similar results. For example, the molecule of C/CPTz-BT which shows the LUMO is delocalized over both the donor and acceptor units had similar wave functions for N/CPTz-BT and Si-CPT-BT. The reason of the delocalization over both the donor and acceptor could be the small dihedral angle of oligomers in Table 4.6. According to Breda's report, slightly better matching of the LUMO energies and small torsion angles provide the delocalization of LUMO over both acceptor and donor units [32].

C/CPTz-BT

HOMO

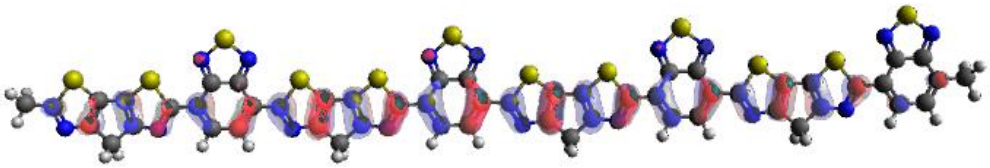

↓

LUMO

N/CPTz-BT

HOMO

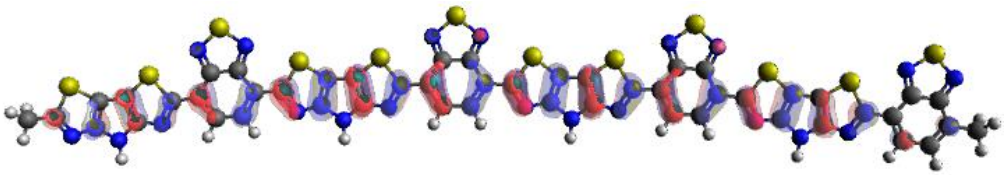

↓

LUMO

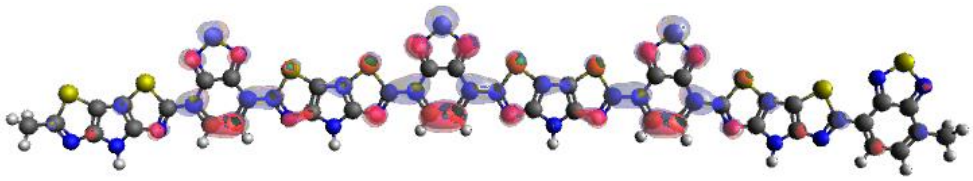

Si/CPTz-BT

HOMO

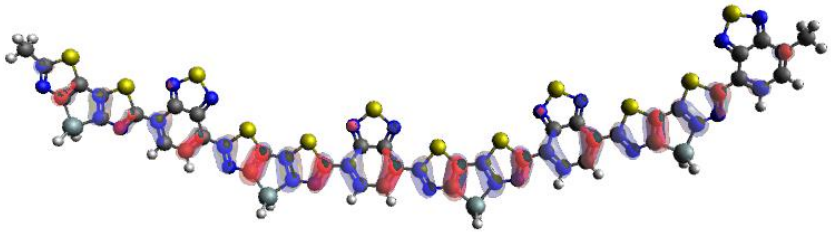

↓

Figure 4.9. Illustrations of the frontier molecular orbitals at B3LYP/6-311G* level of the theory.

LUMO

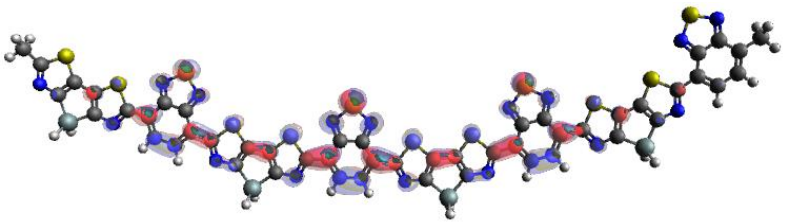

C/DTPn-BT

HOMO

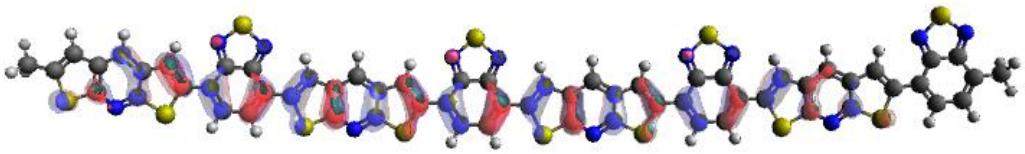

↓

LUMO

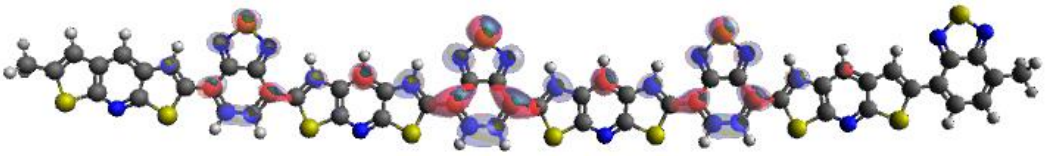

Si/DTPn-BT

HOMO

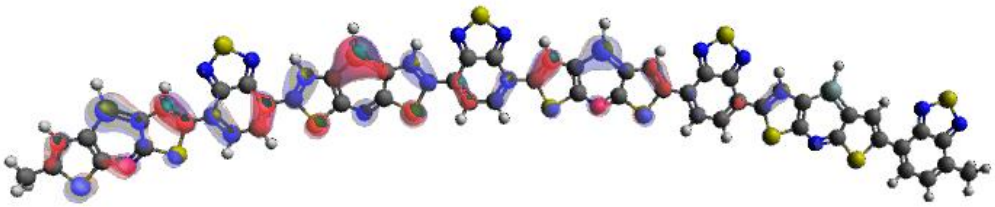

↓

LUMO+2

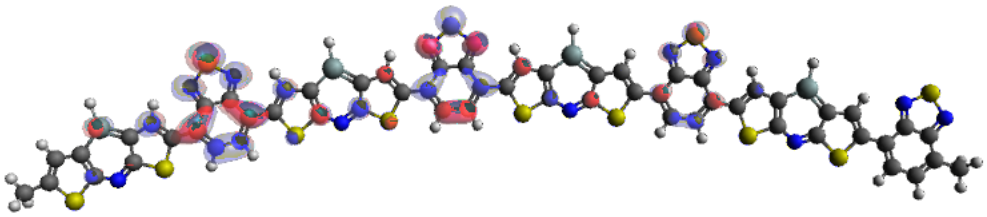

Figure 4.9. Illustrations of the frontier molecular orbitals at B3LYP/6-311G* level of the theory. (cont.)

BDT1-BT

HOMO

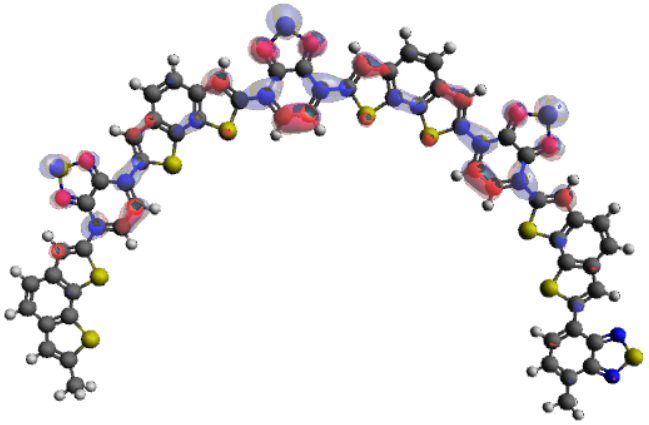

↓

LUMO

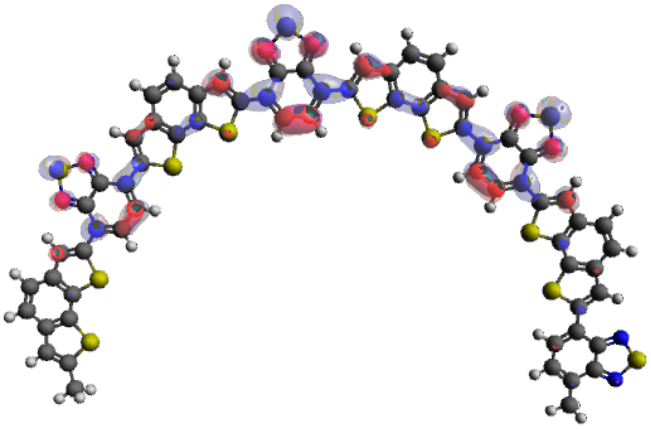

BDT2-BT

HOMO

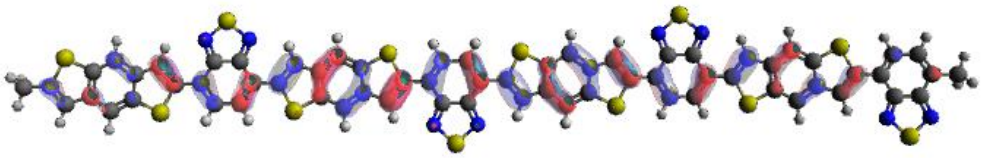

↓

LUMO

Figure 4.9. Illustrations of the frontier molecular orbitals at B3LYP/6-311G* level of the theory. (cont.)

C/CPDP-BT

HOMO

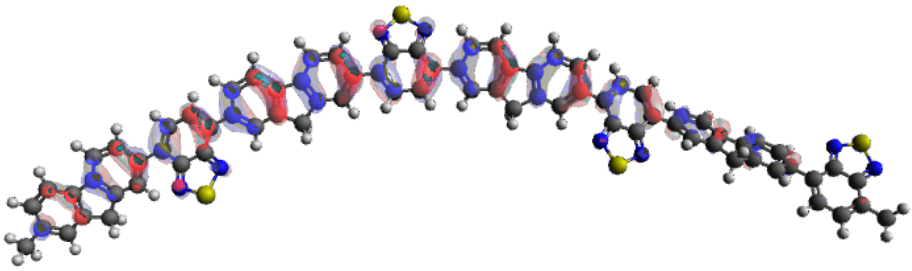

↓

LUMO

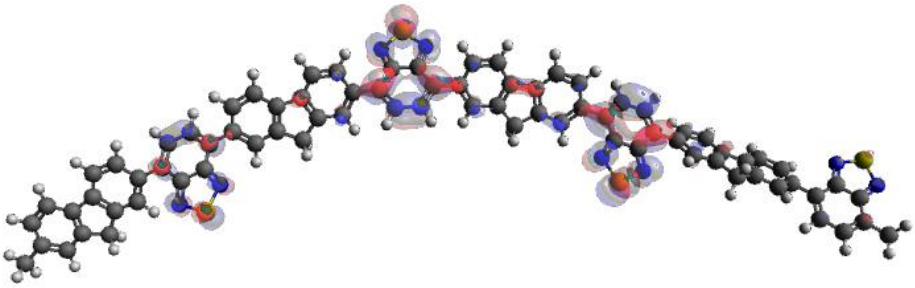

N/CPDP-BT

HOMO

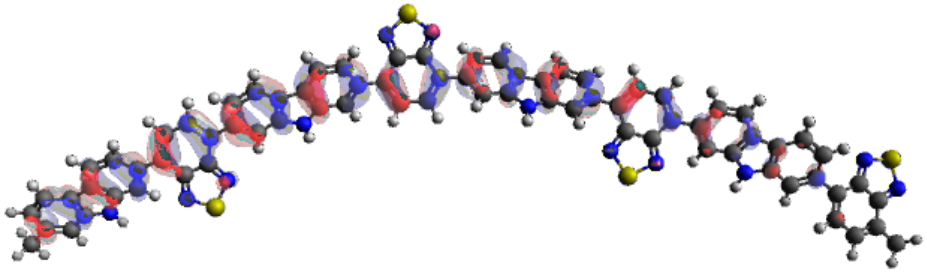

↓

LUMO

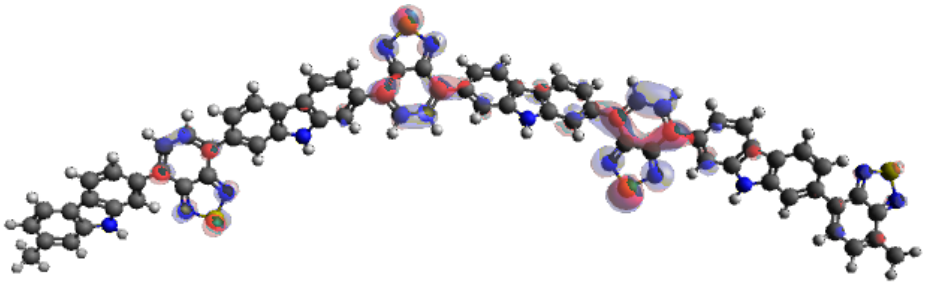

Figure 4.9. Illustrations of the frontier molecular orbitals at B3LYP/6-311G* level of the theory. (cont.)

Si/CPDP-BT

HOMO

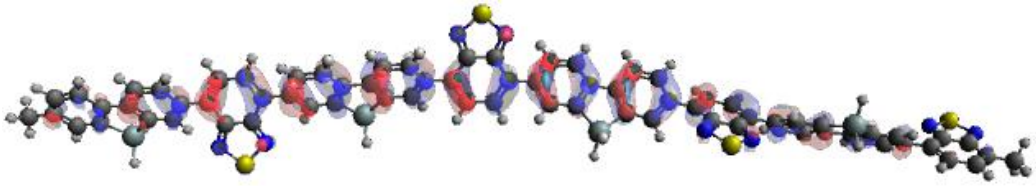

↓

LUMO

C/CPTz-BX

HOMO

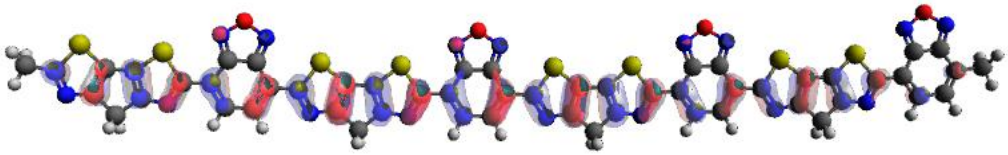

↓

LUMO

N/CPTz-BX

HOMO

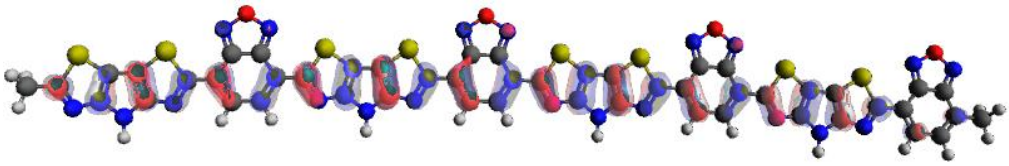

↓

Figure 4.9. Illustrations of the frontier molecular orbitals at B3LYP/6-311G* level of the theory. (cont.)

LUMO

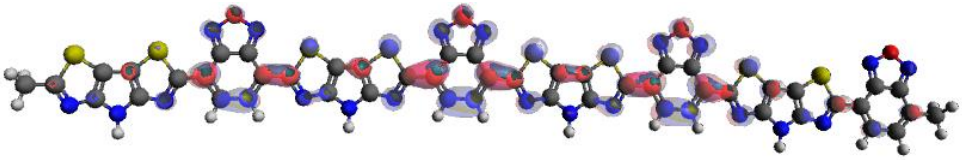

Si/CPTz-BX

HOMO

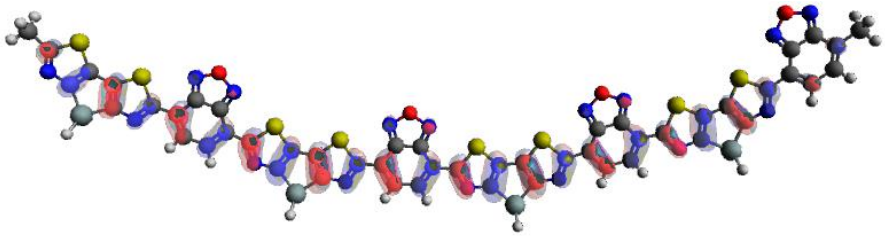

↓

LUMO

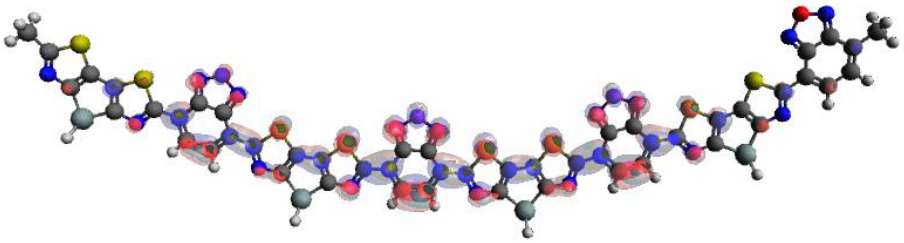

C/DTPn-BX

HOMO

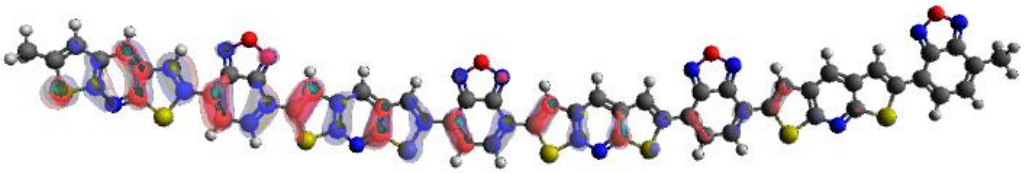

↓

LUMO

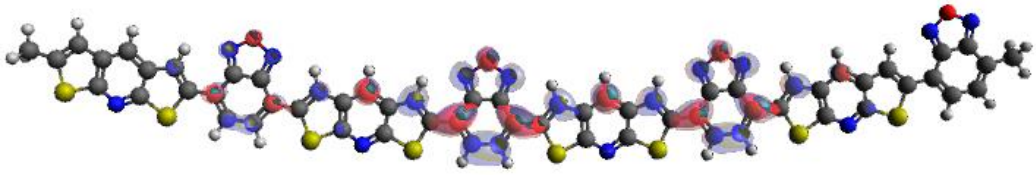

Figure 4.9. Illustrations of the frontier molecular orbitals at B3LYP/6-311G* level of the theory. (cont.)

Si/DTPn-BX

HOMO

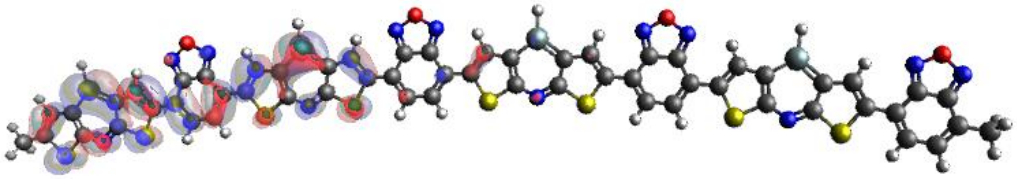

↓

LUMO+2

BDT1-BX

HOMO

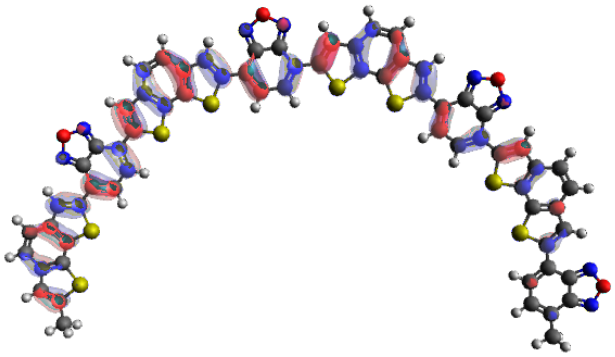

↓

LUMO

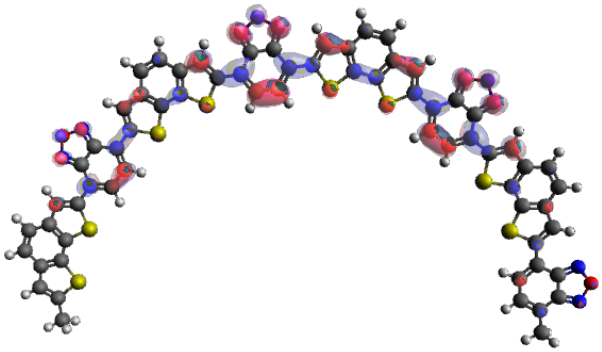

Figure 4.9. Illustrations of the frontier molecular orbitals at B3LYP/6-311G* level of the theory. (cont.)

BDT2-BX

HOMO

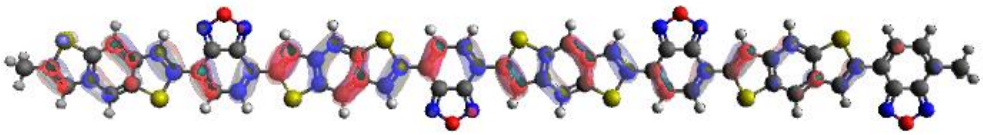

↓

LUMO

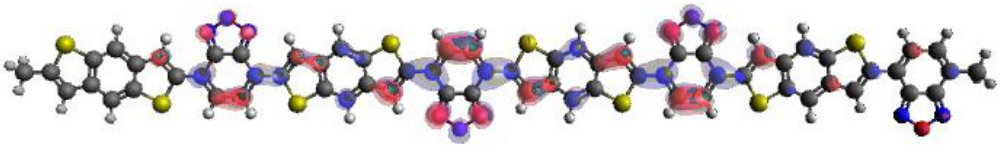

C/CPDP-BX

HOMO

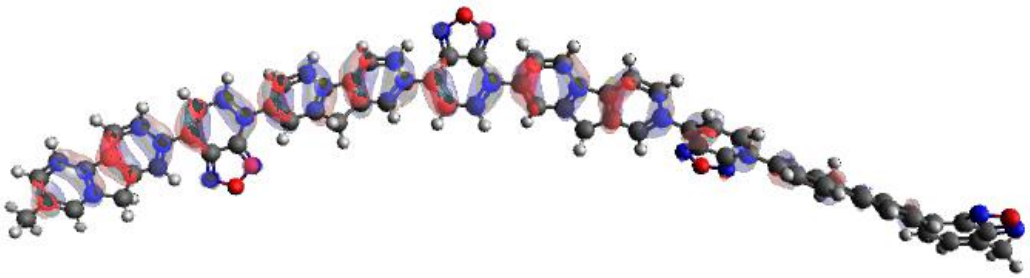

↓

LUMO

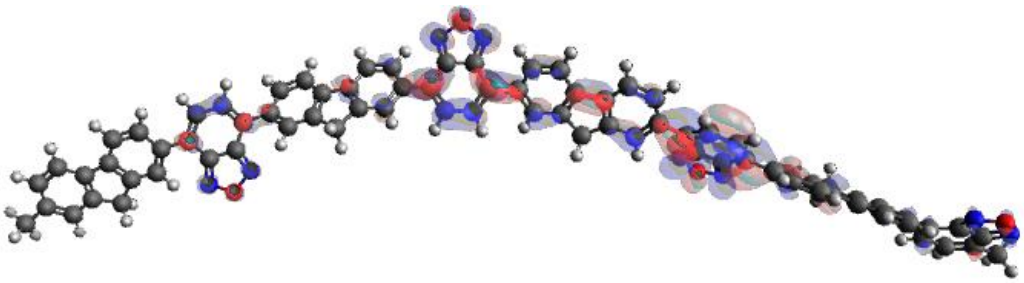

Figure 4.9. Illustrations of the frontier molecular orbitals at B3LYP/6-311G* level of the theory. (cont.)

N/CPDP-BX

HOMO

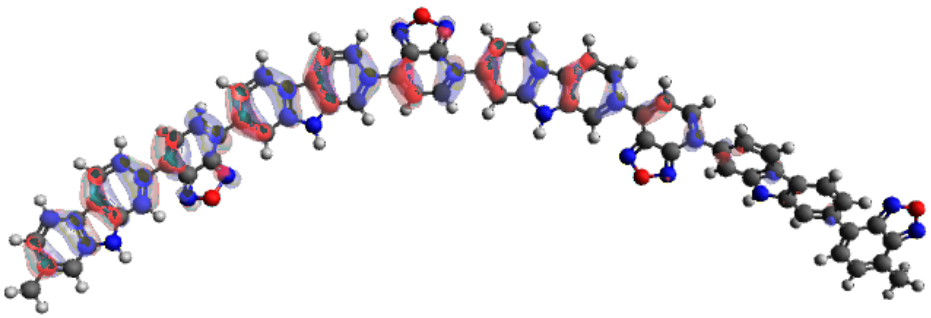

↓

LUMO

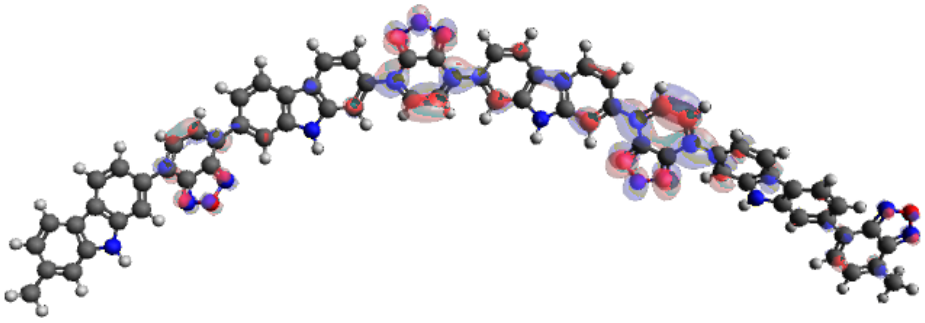

Si/CPDP-BX

HOMO

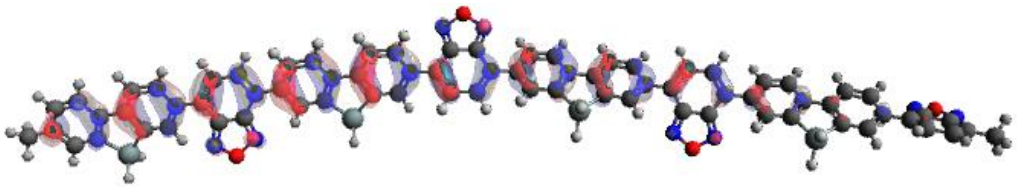

↓

LUMO

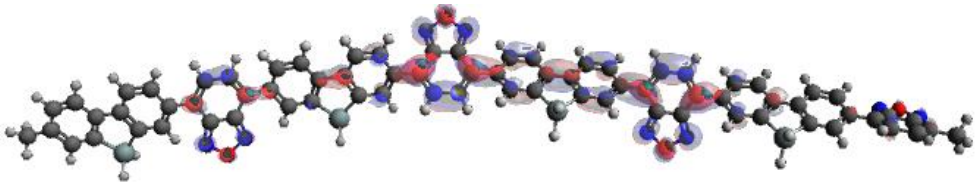

Figure 4.9. Illustrations of the frontier molecular orbitals at B3LYP/6-311G* level of the theory. (cont.)

C/CPTz-BSe

HOMO

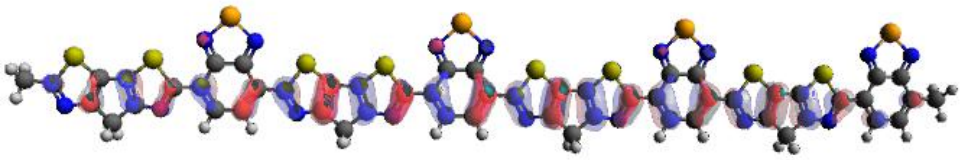

↓

LUMO

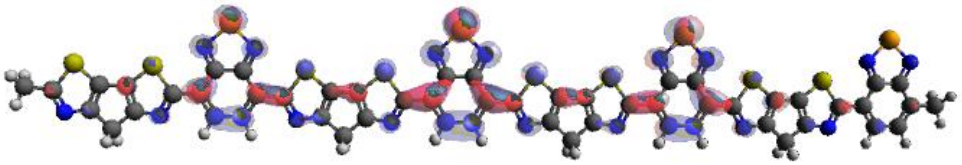

N/CPTz-BSe

HOMO

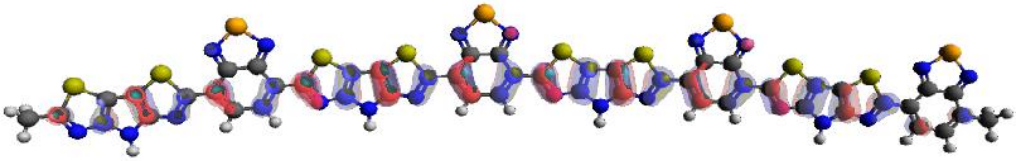

↓

LUMO

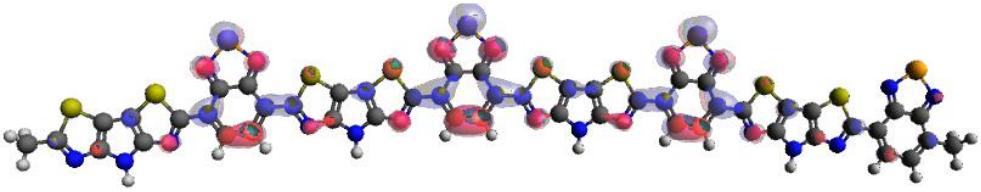

Si/CPTz-BSe

HOMO

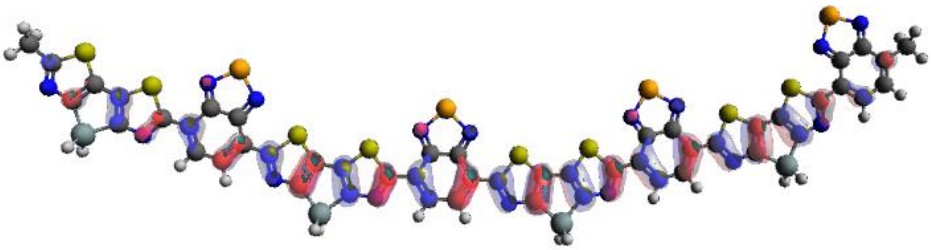

↓

Figure 4.9. Illustrations of the frontier molecular orbitals at B3LYP/6-311G* level of the theory. (cont.)

LUMO

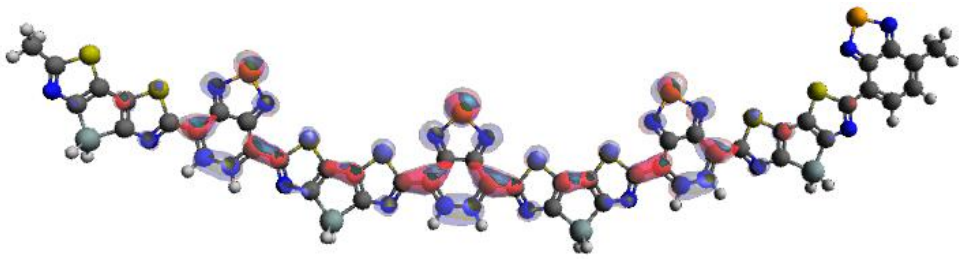

C/DTPn-BSe

HOMO

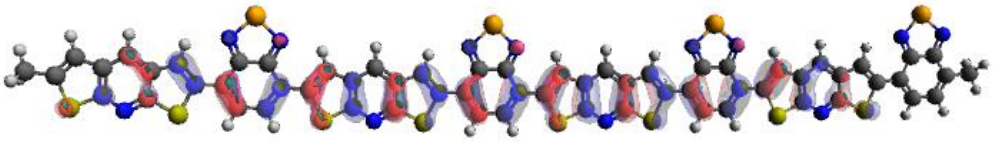

↓

LUMO

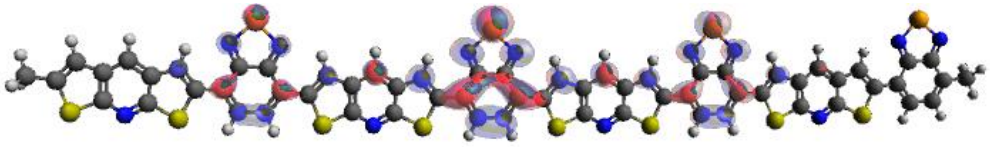

Si/DTPn-BSe

HOMO

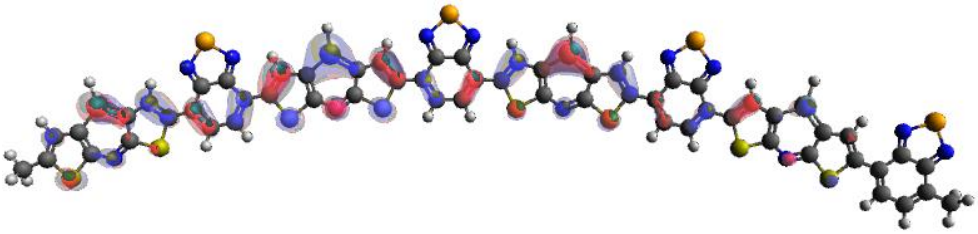

↓

LUMO+2

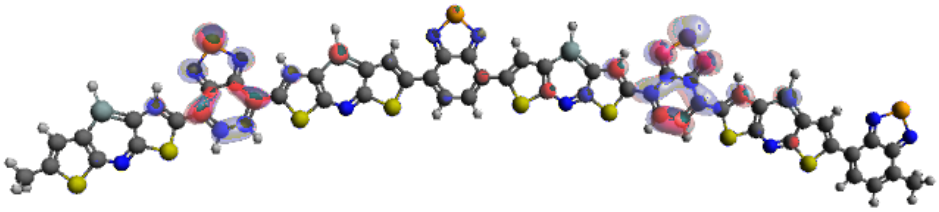

Figure 4.9. Illustrations of the frontier molecular orbitals at B3LYP/6-311G* level of the theory. (cont.)

BDT1-BSe

HOMO

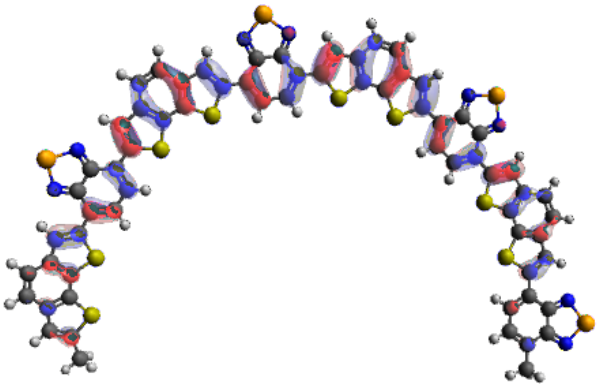

↓

LUMO

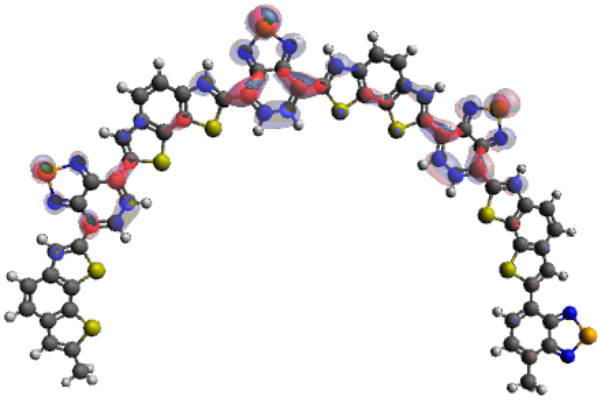

BDT2-BSe

HOMO

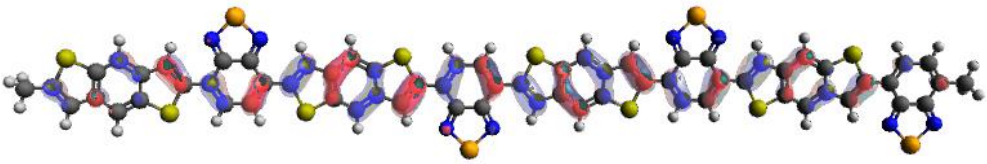

↓

LUMO

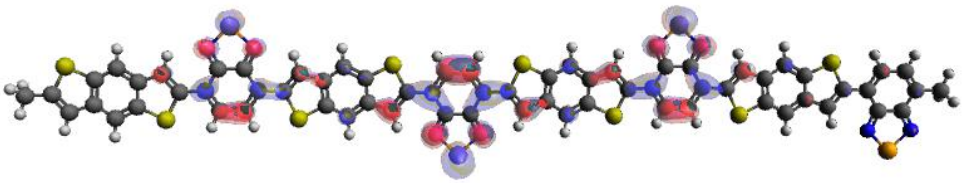

Figure 4.9. Illustrations of the frontier molecular orbitals at B3LYP/6-311G* level of the theory. (cont.)

C/CPDP-BSE

HOMO

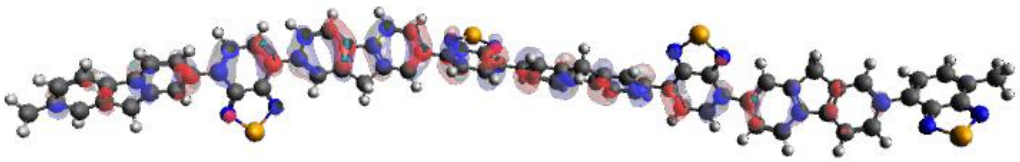

↓

LUMO

N/CPDP-BSE

HOMO

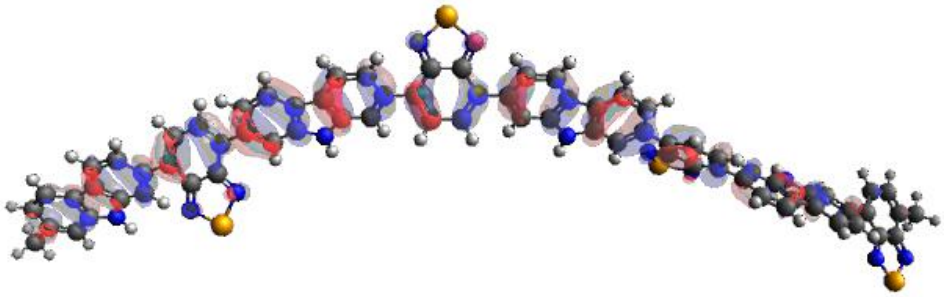

↓

LUMO

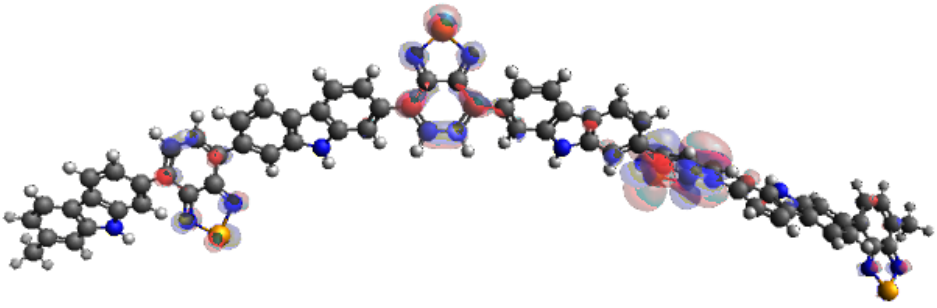

Figure 4.9. Illustrations of the frontier molecular orbitals at B3LYP/6-311G* level of the theory. (cont.)

Si/CPDP-BSE

HOMO

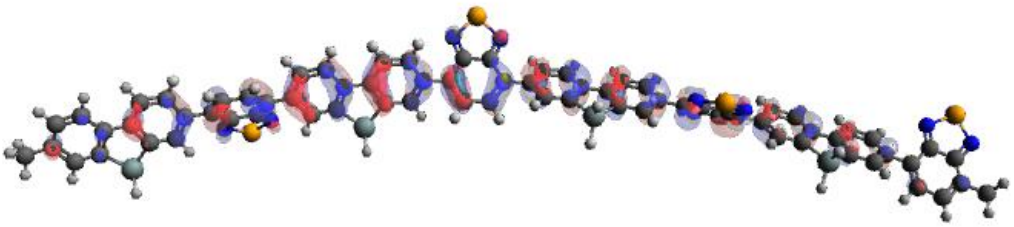

↓

LUMO

C/CPTz-HTAZ

HOMO

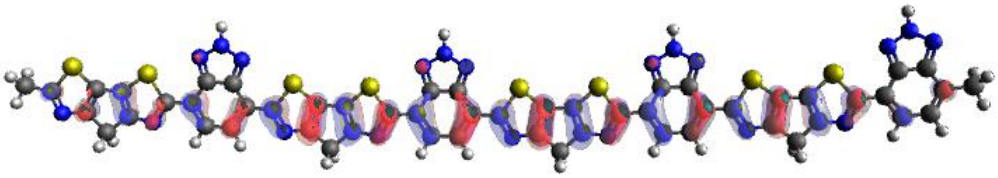

↓

LUMO

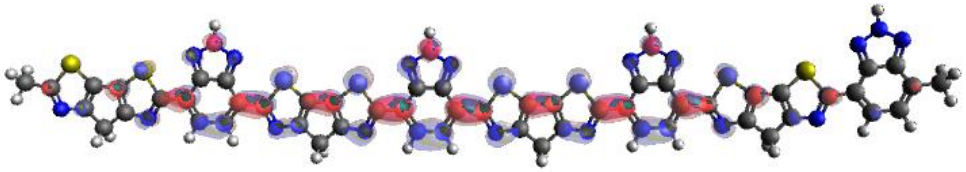

N/CPTz-HTAZ

HOMO

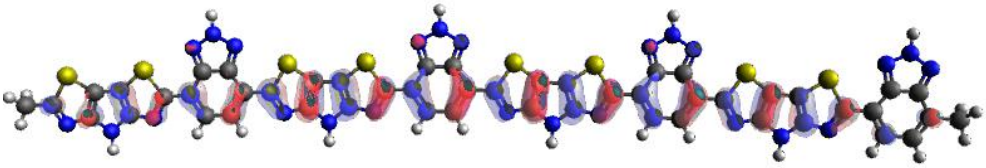

↓

Figure 4.9. Illustrations of the frontier molecular orbitals at B3LYP/6-311G* level of the theory. (cont.)

LUMO

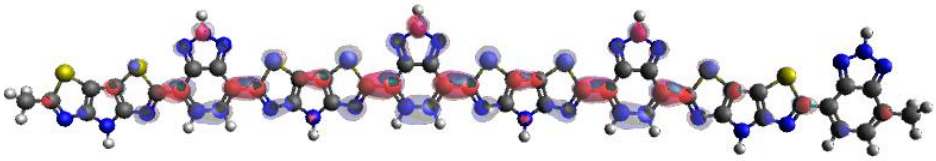

Si/CPTz-HTAZ

HOMO

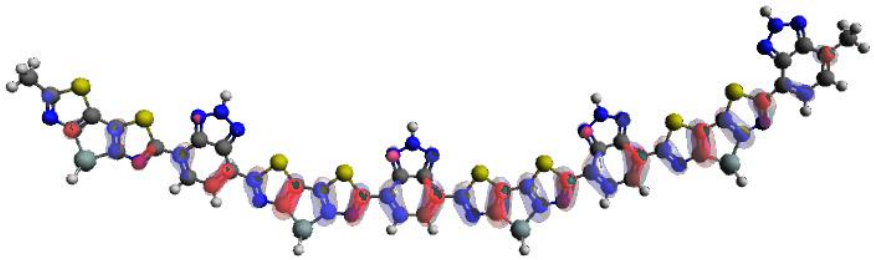

↓

LUMO

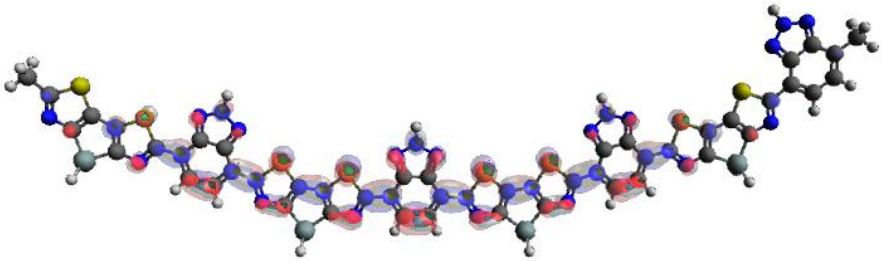

C/DTPn-HTAZ

HOMO

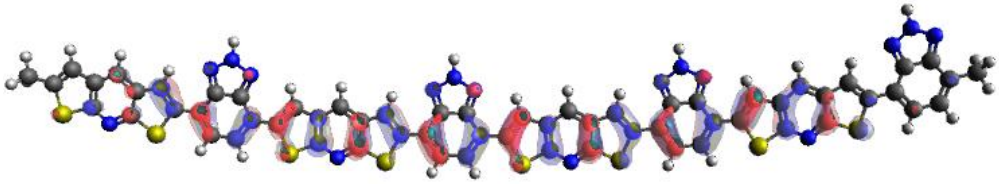

↓

LUMO

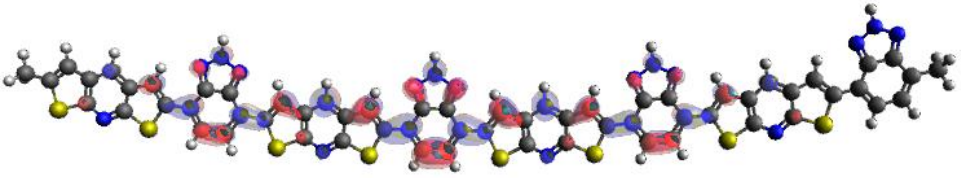

Figure 4.9. Illustrations of the frontier molecular orbitals at B3LYP/6-311G* level of the theory. (cont.)

Si/DTPn-HTAZ

HOMO-2

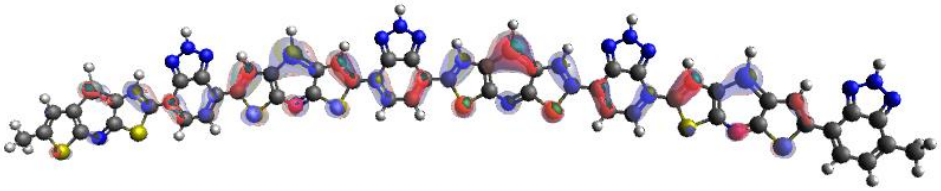

↓

LUMO

BDT1-HTAZ

HOMO

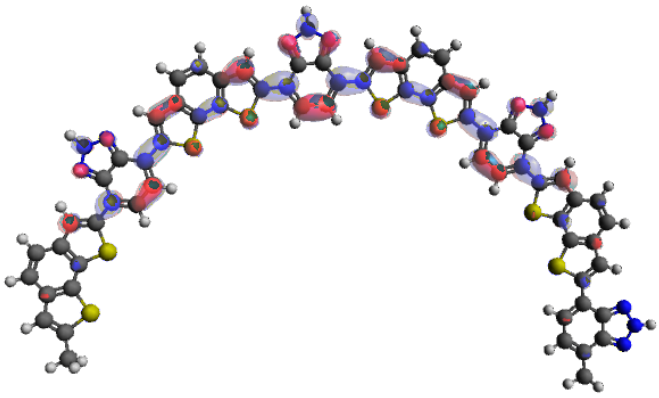

↓

LUMO

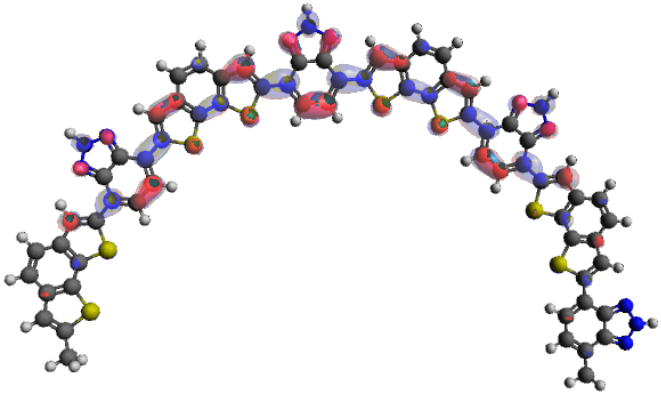

Figure 4.9. Illustrations of the frontier molecular orbitals at B3LYP/6-311G* level of the theory. (cont.)

BDT2-HTAZ

HOMO

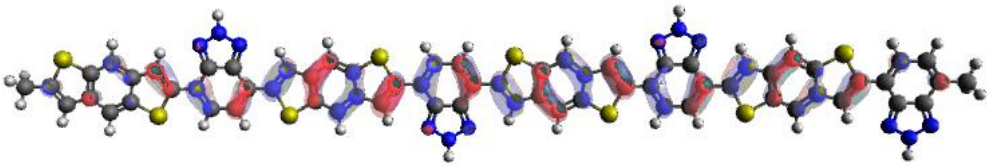

↓

LUMO

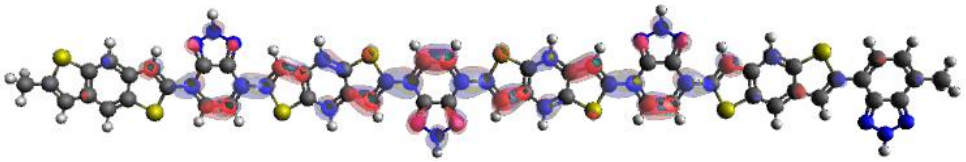

C/CPDP-HTAZ

HOMO

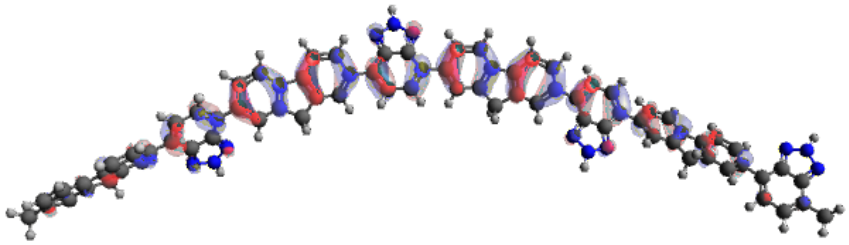

↓

LUMO

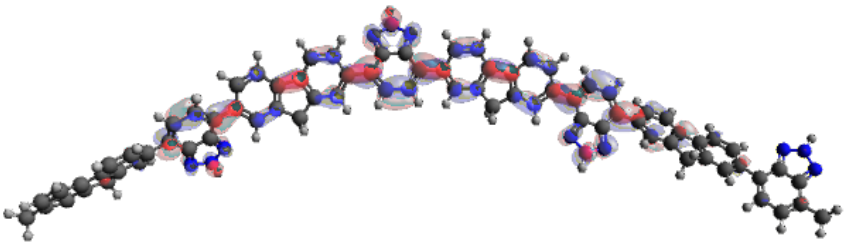

Figure 4.9. Illustrations of the frontier molecular orbitals at B3LYP/6-311G* level of the theory. (cont.)

N/CPDP-HTAZ

HOMO

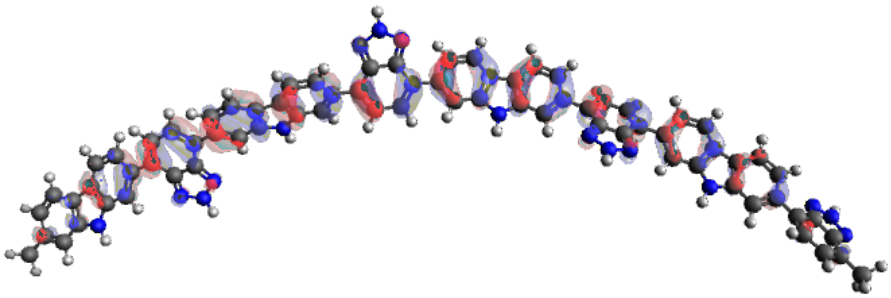

↓

LUMO

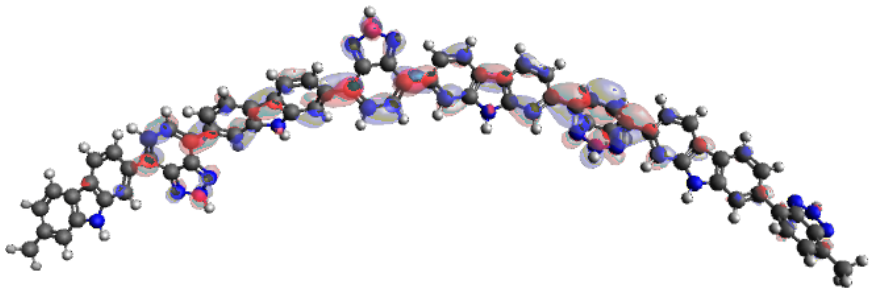

Si/CPDP-HTAZ

HOMO

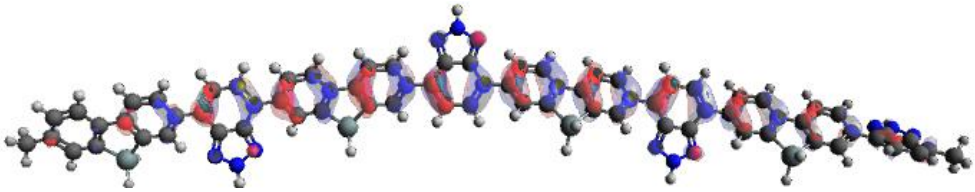

↓

LUMO

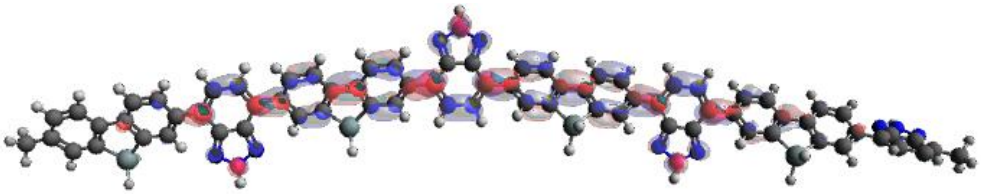

Figure 4.9. Illustrations of the frontier molecular orbitals at B3LYP/6-311G* level of the theory. (cont.)

C/CPTz-QX

HOMO

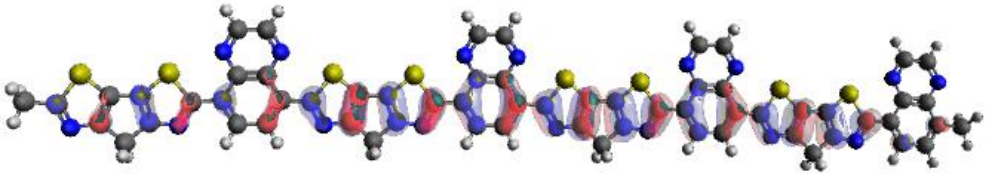

↓

LUMO

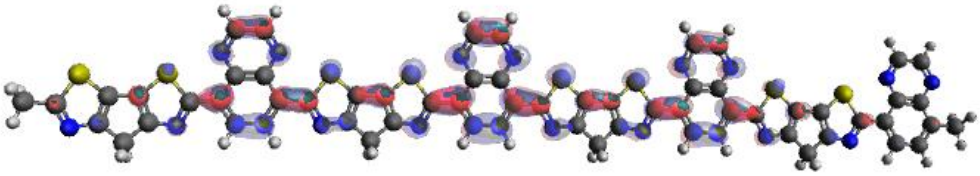

N/CPTz-QX

HOMO

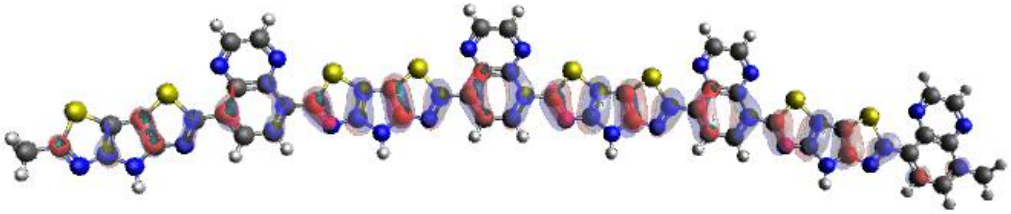

↓

LUMO

Figure 4.9. Illustrations of the frontier molecular orbitals at B3LYP/6-311G* level of the theory. (cont.)

Si/CPTz-QX

HOMO

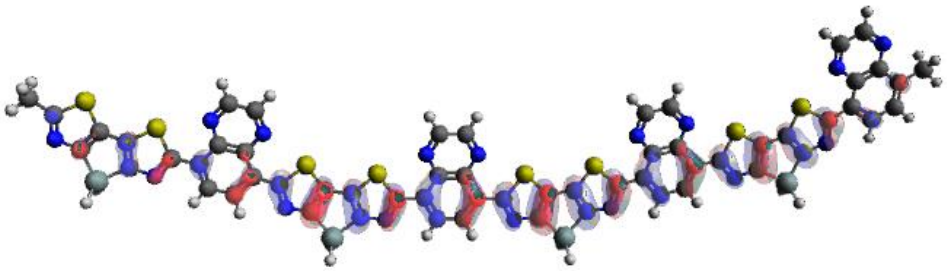

↓

LUMO

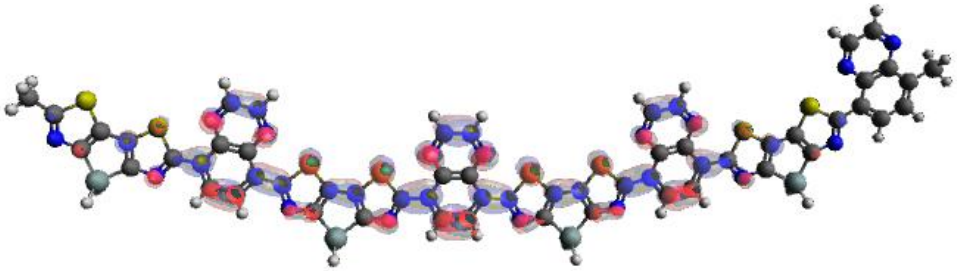

C/DTPn-QX

HOMO

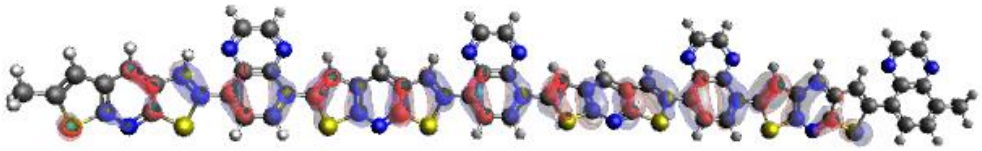

↓

LUMO

Figure 4.9. Illustrations of the frontier molecular orbitals at B3LYP/6-311G* level of the theory. (cont.)

Si/DTPn-QX

HOMO

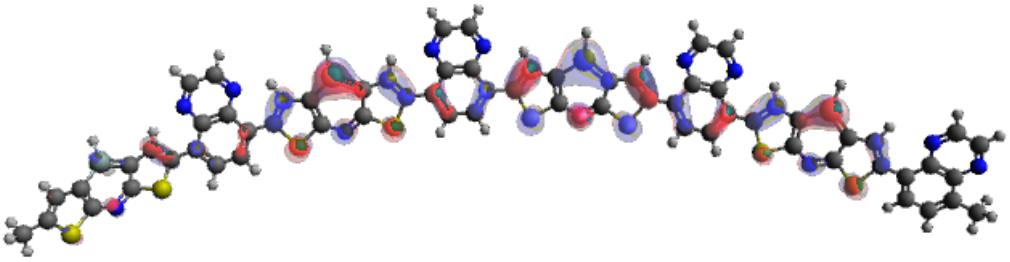

↓

LUMO

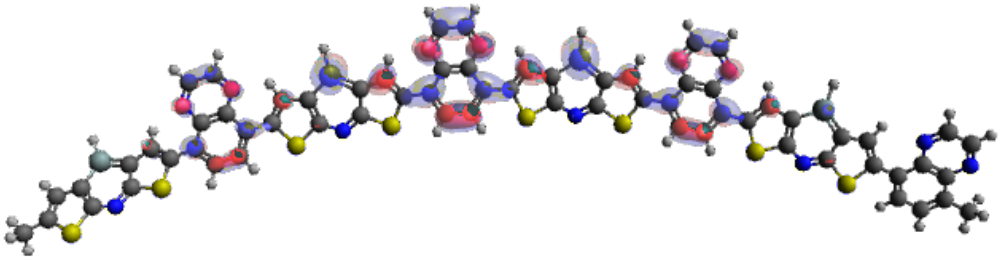

BDT1-QX

HOMO

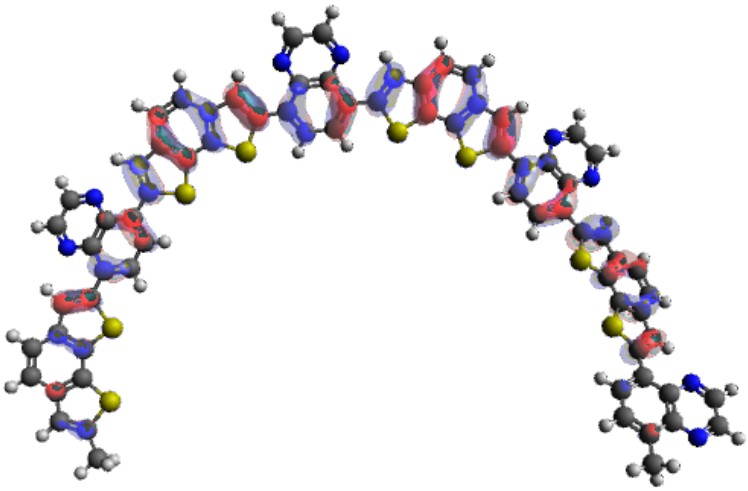

↓

Figure 4.9. Illustrations of the frontier molecular orbitals at B3LYP/6-311G* level of the theory. (cont.)

LUMO

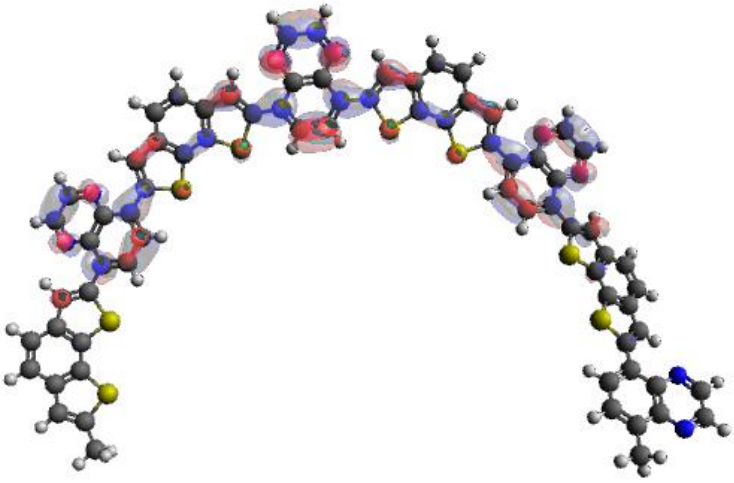

BDT2-QX

HOMO

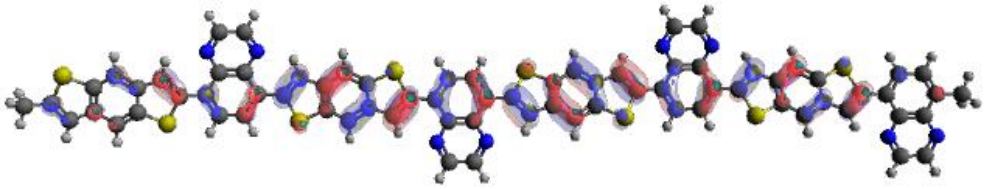

↓

LUMO

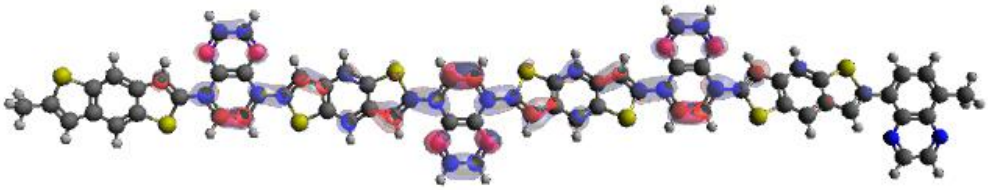

C/CPDP-QX

HOMO

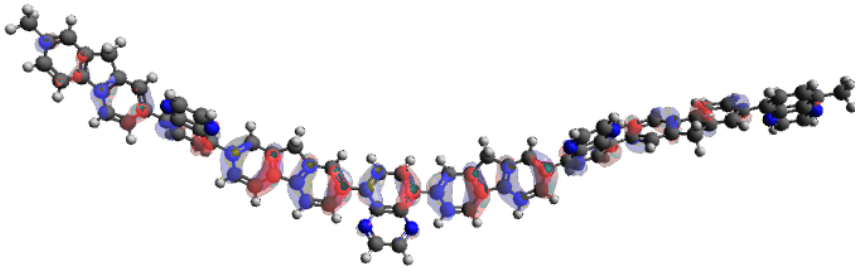

↓

Figure 4.9. Illustrations of the frontier molecular orbitals at B3LYP/6-311G* level of the theory. (cont.)

LUMO

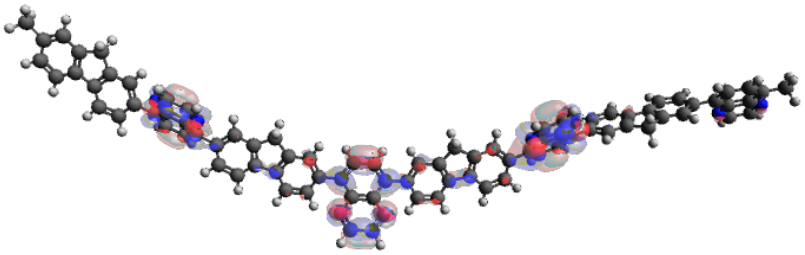

N/CPDP-QX

HOMO

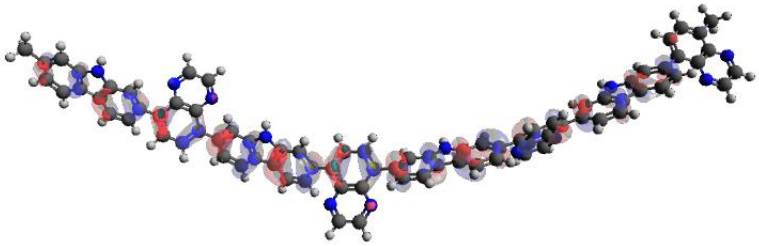

↓

LUMO

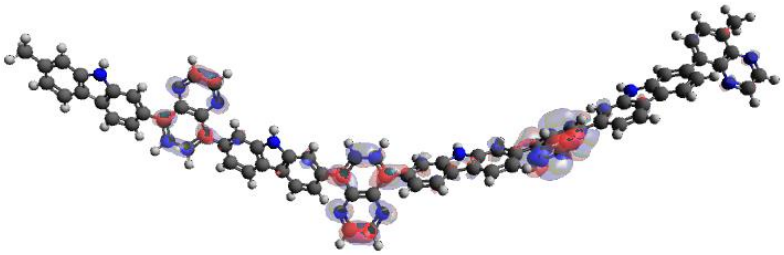

Si/CPDP-QX

HOMO

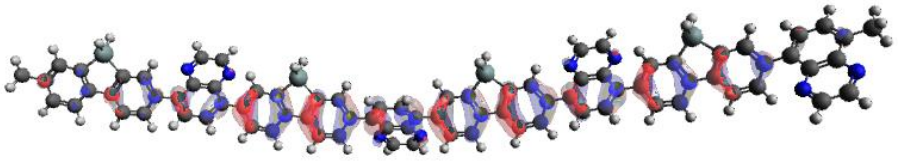

↓

LUMO

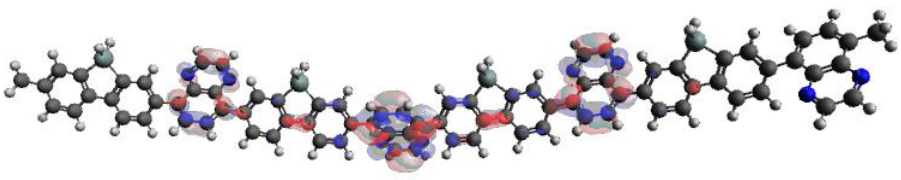

Figure 4.9. Illustrations of the frontier molecular orbitals at B3LYP/6-311G* level of the theory. (cont.)

4.9. Calculation of Open Circuit Voltages

The open circuit voltage is an important parameter to determine the power conversion efficiency. When the open circuit voltage increases, the power conversion efficiency increases. Thus, more electrons can be transferred from the donor to the acceptor [10].

Open circuit voltages of the oligomers are calculated according to the Scharber Method by the following formula [18]. In this formula, the LUMO of the PCBM is taken as -4.1 eV, e represents the elementary charge and the value of 0.3 V is an empirical factor. Calculated open circuit voltages of oligomers are shown in table 4.13. The molecule of C/DTPn-BX has the highest value of open circuit voltage (2.10 V) and the molecule of N/CPTz-BSe has the lowest value (0.85 V) compared to the others.

$$V_{OC} = (1/e)(|E^{Donor}\text{HOMO}| - |E^{PCBM}\text{LUMO}|) - 0.3\,V \qquad (4.1)$$

Table 4.13. Open circuit voltages (V_{oc}) of the molecules (V) (B3LYP/6-311G*).

Donor - Acceptor				
	BT	BX	BSe	HTAZ
C/CPTz	1.01	1.29	0.92	0.94
N/CPTz	0.94	1.23	0.85	0.87
Si/CPTz	1.25	1.52	1.17	1.19
C/DTPn	1.03	2.10	1.69	1.74
Si/DTPn	1.41	1.72	1.33	1.48
BDT1	1.21	1.50	1.14	1.12
BDT2	1.22	1.48	1.04	1.15
C/CPDP	1.49	1.76	1.50	1.36
N/CPDP	1.12	1.65	1.43	1.35
Si/CPDP	1.67	1.93	1.67	1.52

4.8. Choice of Molecules for Photovoltaic Materials

There are four important criteria, which are HOMO, LUMO, optical band gap and reorganization energies, to determine suitable molecules in organic solar cells. First, the

HOMO of the donor should be at least 0.3 eV higher than the HOMO of the acceptor of PCBM which is -6.0 eV. In addition, the value of HOMO of the donors should be over the air oxidation threshold which is known as 5.27 eV. Thus, the range of HOMO of the donors is between -5.27 eV and -5.7 eV. Second, the LUMO of the donor should be at least 0.3 higher than the LUMO of the acceptor of PCBM which is -4.1 eV. Therefore, the LUMO level of the donors is higher than -3.8 eV. Third, optical band gap energies should be between 1.4 eV to 1.9 eV to obtain suitable phovoltaic materials. Finally, reorganization energies of the donors should be low to ensure higher charge transfer rate and higher charge mobility.

In this study, bond length alternations and distortion energies are used as indicators. LUMO levels of all molecules are higher than -3.8 eV with low reorganization energies. Therefore, the LUMO level of the donor and the reorganization energy are not important criteria to choose molecules for this study. HOMO levels and optical band gap energies of the oligomers were important factors to determine suitable materials. The best compounds for photovoltaic materials among a class of oligomers were shown with (*) in Table 4.14. 16 out of 50 oligomers are found as suitable materials to use in organic solar cells. The donors of BDT1, BDT2, CPTz and their derivatives showed better results than the others.

Table 4.14. Suitable compounds for photovoltaic materials.

Donor - Acceptor				
BT	BX	BSe	HTAZ	QX
C/CPTz*	C/CPTz*	C/CPTz	C/CPTz*	C/CPTz*
N/CPTz*	N/CPTz*	N/CPTz	N/CPTz*	N/CPTz*
Si/CPTz*	Si/CPTz	Si/CPTz*	Si/CPTz*	Si/CPTz*
C/DTPn	C/DTPn	C/DTPn	C/DTPn	C/DTPn
Si/DTPn	Si/DTPn	Si/DTPn	Si/DTPn	Si/DTPn
BDT1*	BDT1	BDT1*	BDT1	BDT1
BDT2*	BDT2	BDT2*	BDT2	BDT2
C/CPDP	C/CPDP	C/CPDP	C/CPDP	C/CPDP
N/CPDP	N/CPDP	N/CPDP	N/CPDP	N/CPDP
Si/CPDP	Si/CPDP	Si/CPDP	Si/CPDP	Si/CPDP

5. CONCLUSION

Geometric and optical properties of a group of donor-acceptor oligomers were investigated computationally. The effect of side chain and the chain length were examined. Thanks to Benchmark calculations which contain five different models, HOMO, LUMO energies and optical band gaps were calculated so, accurate results were obtained with the correct methodology. The number of the donors increased from 5 to 10 with the heteroatom substitution thus, the effect of heteroatom was examined.

16 oligomers were determined as suitable materials in 50 molecules according to four important criteria which contain low reorganization energy, LUMO energy higher than -3.8 eV, HOMO energy range between -5.27 eV and -5.7 eV and the optical band gap between 1.4 eV and 1.9 eV. In this study, the donors of BDT1, BDT2, CPTz and their derivatives have shown the best performance. Overall, a suitable computational method to discriminate oligomers for photovoltaic cells has been proposed.

REFERENCES

1. Ossai, C. I., "Optimal renewable energy generation – Approaches for managing ageing assets mechanisms", *Renewable and Sustainable Energy Reviews*, Vol. 72, pp. 269–280, 2017.

2. Foster, E., Contestabile, M., Blazquez, J., Manzano, B., Workman, M., Shah, N., "The unstudied barriers to widespread renewable energy deployment: Fossil fuel price responses", *Energy Policy*, Vol. 103, pp. 258–264, 2017.
3. Miles, R. W., Zoppi, G., Forbes, I., "Inorganic photovoltaic cells", *Materialstoday*, Vol. 10, No. 11, pp. 20-27, 2007.

4. Mekemeche, A., Beghdad, M., Belarbi, M., Semmache, B., Cuminal, Y., "Two dimensional device simulation and performance optimization of n-type silicon solar cell structure using PC2D", *Solar Energy*, Vol. 146, pp. 119-124, 2017.

5. Salavei, A., Menossi, D., Piccinelli, F., Kumar, A., Mariotto, G., Barbato, M., Meneghini, M., Meneghesso, G., Mare, S. D., Artegian, E., Romeo, A., "Comparison of high efficiency flexible CdTe solar cells on different substrates at low temperature deposition", *Solar Energy*, Vol. 139, pp. 13-18, 2016.

6. Moradi, M., Teimouri, R., Saadat, M., Zahedifar, M., "Buffer layer replacement: A method for increasing theconversion efficiency of CIGS thin film solar cells", *Optik*, Vol. 136, pp. 222-227, 2017.

7. Che, H., Liu, X., Gao, Y., Liu, J., Cao, Z., "Hydrothermal electrochemical deposition synthesis $NiSe_2$ as efficient counter electrode materials for dye-sensitized solar cells", *Journal of Alloys and Compounds*, Vol. 705, pp. 645-651, 2017.

8. Lin, W. K., Su, S. H., Yeh, M. C., Chen, C. Y., Yokoyama, M., "Enhancing efficiency of perovskite solar cells using a thin buffer layer", *Vacuum*, Vol. 140, pp. 82-88, 2017.

9. Bagher, A. M., "Comparison of organic solar cells and inorganic solar cells", *International Journal of Renewable and Sustainable Energy*, Vol. 3, No.3, pp. 53-58, 2014.

10. Liu, X., He, R., Shen, W., Li, M., "Molecular design of donor-acceptor conjugated copolymers based on C-, Si- and N-bridged dithiophene and thienopyrroledione derivatives units for organic solar cells", *Journal of Power Sources*, Vol. 245, pp. 217-223, 2014.

11. Bagher, A. M., "Introduction to Organic Solar Cells", *Sustainable Energy*, Vol. 2, No. 3, pp. 85-90, 2014.

12. Zhou, H., Yang, L., You, W., "Rational Design of High Performance Conjugated Polymers for Organic Solar Cells", *Macromolecules*, Vol. 45, pp. 607-632, 2012.

13. Chidichimo, G., Filippelli, L., "Organic Solar Cells: Problems and Perspectives", *International Journal of Photoenergy*, Vol. 2010, pp. 1-11, 2010.

14. Cheng, Y. J., Yang, S. H., Hsu, C. S., "Synthesis of Conjugated Polymers for Organic Solar Cell Applications", *Chemical Reviews*, Vol. 109, No. 11, pp. 5868–5923, 2009.

15. Bundgaard, E., Krebs, F. C., "Low band gap polymers for organic photovoltaics", *Solar Energy Materials & Solar Cells*, Vol. 91, pp. 954–985, 2007.

16. Kim, Y., Yoo, D., Jang, J., Song, Y., Jeong, H., Cho, K., Hwang, W.-T., Lee W., Kim, T.-W., Lee, T., "Characterization of PI:PCBM organic nonvolatile resistive memory devices under thermal stress", *Organic Electronics*, Vol. 33, pp. 48-54, 2016.

17. Li, Z., Qiao, Z., Liu, W., Wang, Z., Wang, H., Shi, F., "Conjugated random copolymer of benzodithiophene-difluorobenzene-diketopyrrolopyrrole-benzothiadiazole with abroad absorption range of 300–900 nm for bulk heterojunction solar cells", *Materials Letters*, Vol. 139, pp. 307-310, 2015.

18. Scharber, M. C., Mühlbacher, D., Koppe, M., Denk, P., Waldauf, C., Heeger, A. J., Brabec, C. J., "Design Rules for Donors in Bulk-Heterojunction Solar Cells—Towards 10% Energy-Conversion Efficiency", *Advanced Materials*, Vol. 18, pp. 789-794, 2006.

19. Yohannes, T., Zhang, F., Svensson, M., Hummelen, J. C., Andersson, M. R., Inganäs, O., "Polyfluorene copolymer based bulk heterojunction solar cells", *Thin Solid Films*, Vol. 449, pp. 152–157, 2004.

20. Fitzner, R., Reinold, E., Mishra, A., M. Osteritz, E., Ziehlke, H., Körner, C., Leo, K., Riede, M., Weil, M., Tsaryova, O., Weiß, A., Uhrich, C., Pfeiffer, M., Bäuerle, P., "Dicyanovinyl-Substituted Oligothiophenes: Structure–Property Relationships and Application in Vacuum- Processed Small-Molecule Organic Solar Cells", *Advanced Functional Materials*, Vol. 21, pp. 897–910, 2011.

21. Walker, B., Kim, C., Nguyen, T. Q., "Small Molecule Solution-Processed Bulk Heterojunction Solar Cells", *Chemistry of Materials*, Vol. 23, pp. 470-482, 2011.

22. Parr, R. G., Weitao, T., "*Density Functional Theory of Atoms and Molecules*", Oxford University Press, 1989.

23. Becke, A. D., "A New Mixing of Hartree–Fock and Local Density Functional Theories", *The Journal ofChemical Physics*, Vol. 98, No. 2, pp. 1372-1377, 1993.

24. Becke, A. D., "Density Functional Exchange Energy Approximation with Correct Asymptotic Behavior",*Physical Review A*, Vol. 38, No. 6, pp. 3098–3100, 1988.

25. Roos, B. O., "*Lecture Notes in Quantum Chemistry II"*, vol. 64. Springer Berlin

Heidelberg, 1994.

26. Leach, A. R., "*Molecular Modelling. Principles and Applications (2nd Edition) by Andrew R. Leach*", Prentice Hall, 2001.

27. Lee, C., Weitao, Y., Parr, G. R., "Development of the Colle-Salvetti CorrelationEnergy Formula into a Functional of the Electron Density", *Physical Review B*, Vol. 37, No. 2, pp. 785–789, 1988.

28. Becke, A. D., "Density Functional Thermochemistry. III. The role of exact exchange",*The Journal of Chemical Physics,*Vol. 98, pp. 5648-5652, 1993.

29. Pauling, L., "The Nature ofthe Chemical Bond. IV. The Energyof Single Bonds and the Relavitve Electronegativity of Atoms", *Journal of the American Chemical Society*, Vol. 54, No. 9, pp. 3570–3582, 1932.

30. Coropceanu, V., Cornil, J., Filho, D. A., Olivier, Y., Silbey, R., Brédas J L., "Charge Transport in Organic Semiconductors" *Chemical Reviews,* Vol. 107, No. 4, pp. 926-952,2007.

31. Oshi, R., Abdalla S., Springborg M., "Study of the influence of functionalization on the reorganization energy of naphthalene using DFT", *Computational and Theoretical Chemistry*, Vol. 1099, pp. 209-215, 2017.

32. Pandey, L., Risko, C., Norton J. E., Brédas J.-L., "Donor−Acceptor Copolymers of Relevance for Organic Photovoltaics: A Theoretical Investigation of the Impact of Chemical Structure Modifications on the Electronic and Optical Properties", *Macromolecules*, Vol. 45, pp. 6405−6414, 2012.

33. Marder, S. R., Perry, J. W., Bourhill, G., Gorman, C. B., Tiemann, B. G., Mansour K., "Relation Between Bond-Length Alternation and Second Electronic Hyperpolarizability of Conjugated Organic Molecules", *Science*, Vol. 261, No. 5118, pp. 186-189, 1993.

34. Meyers, F., Marder, S. R., Pierce, B. M., Brédas J. L., "Electric Field Modulated Nonlinear Optical Properties of Donor- Acceptor Polyenes: Sum-Over-States Investigation of the Relationship between Molecular Polarizabilities (α, β, and γ) and Bond Length Alternation", *Journal of American Chemical Society*, Vol. 116, No.23, pp. 10703-10714, 1994.

35. McCormick, T. M., Bridges, C. R., Carrera, E. I., DiCarmine, P. M., Gibson, G. L., Hollinger, J., Kozycz, L. M., Seferos, D. S., "Conjugated Polymers: Evaluating DFT Methods for More Accurate Orbital Energy Modeling", *Macromolecules*, Vol. 46, No. 10, pp. 3879–3886, 2013.

36. Risko, C., McGehee, M. D., Brédas, J.-L., "A quantum-chemical perspective into low optical-gap polymers for highly-efficient organic solar cells", *Chemical* Science, Vol. 7, pp. 1200–1218, 2011.

37. Hutchison, G. R., Ratner M. A., Marks T. J., "Hopping Transport in Conductive Heterocyclic Oligomers: Reorganization Energies and Substituent Effects", *Journal of American Chemical Society*, Vol. 127, pp. 2339-2350, 2005.

38. Liang, Y., Xu Z., Xia J., Tsai S.-T., Wu Y., Li G., Ray C., Yu L., "For the Bright Future—Bulk Heterojunction Polymer Solar Cells with Power Conversion Efficiency of 7.4%", *Advanced Energy Materials*, Vol. 22, pp. E135–E138, 2010.

39. Shockley, W., Queisser, H. J., "Detailed Balance Limit of Efficiency of P- n Junction Solar Cells", *Journal of Appied Physics*, Vol. 32, No.3, pp. 510–519, 1961.

40. Genene, Z., Wang, J., Meng, X., Ma, W., Xu, X., Yang, R., Mammo, W., Wang, E., "High Bandgap (1.9 eV) Polymer with Over 8% Efficiency in Bulk Heterojunction Solar Cells", *Advanced Electronic Mateials*, Vol. 2, No. 1600084, pp. 1-7, 2016.

41. Wakim, S., Aïch, B.-R., Tao, Y., Leclerc M., "Charge Transport, Photovoltaic, and Thermoelectric Properties of Poly(2,7- Carbazole) and Poly(Indolo[3,2- b] Carbazole) Derivatives", *Polymer Reviews*, Vol. 48, No.3, pp. 432-462, 2008.

42. Hutchison, G.R., Campbell, C.M., O'Boyle, N.M., "Computational Design and Selection of Optimal Organic Photovoltaic Materials", *Journal of Physical Chemistry C*, Vol. 115, pp. 16200–16210, 2011.

43. Baran, D., Kirchartz, T., Wheeler, S., Dimitrov, S., Abdelsamie, M., Gorman, J., Ashraf, R. S., Holliday, S., Wadsworth, A., Gasparini, N., Kaienburg, P., Yan, H., Amassian, A., Brabec, C. J., Durrant, J. R., McCulloch I., "Reduced voltage losses yield 10% efficient fullerene free organic solar cells with >1 V open circuit voltages", *Energy & Environmental Science*, Vol. 9, pp. 3783-3793, 2016.